Response to Reviewers

We copy in the reviewer's comments and critique in blue and provide our response in **black boldface**. In gray we copied in our final author responce for reference. This allows us to provide a short response (in black) whenever we were able to do our revisions as foreseen in our final author response. We begin each response with a page and line number or range of line numbers that relate to the track changes manuscript as the reference.

During the revisions we also revised a few minor passages where we found the need for an improved wording, even when none of the reviewers was critical about it.

We hope that with these changes our manuscript can now be accepted as final paper in ACP. We thank both reviewers for the very careful and supportive assessment.

Reviewer 1

Reviewer: This paper reports the effect of the solar eclipse in March 2015 on a network of measurement sites in Switzerland. The effects of topology are relevant for this region, and this is probably the most comprehensive study of eclipse meteorology over a multi-altitude network to date. The authors seem particularly interested in comparing two versions of the "cold cored cyclone" as presented by Clayton and modified by Aplin and Harrison, since the trajectory of the 2015 eclipse makes Switzerland ideal for such a test. Altogether this is a thorough and competent study, at a higher standard than many eclipse meteorology papers, and I am happy to recommend publication with some minor revisions.

Author Response: Thank you very much for this positive assessment.

Reviewer: The main concern I have is to do with the structure of the paper. The authors present their data analysis methods before describing the data analysis itself and this makes for a disjointed read. For a journal that doesn't use a "methods" section like ACP I would recommend moving the specific analysis techniques to the section on, for example, analysing temperature effects (or whatever it is).

Author Response: This can be done. We suggest to move the contents of Sections 2.3–2.8 in the discussion version to the respective paragraph where the results are presented (this is what this reviewer recommends in the detailed feedback below).

P5/L14–P6/L21: The information in these sections was moved to the respective results sections: P8/L2–8; P9/L21–25; P8/L26–33; P11/L11–12; P7/L28–32; P9/L9–14.

Reviewer: Occasionally the data analysis decisions do not appear to have any theoretical basis, for example, the choice of a gamma distribution for the temperature changes, and perhaps also the diurnal variation in the diffuse fraction. The gamma distribution is justified by the authors because it permits others to see their measured temperature changes in context, however this could be achieved with a cumulative probability distribution to all the data, without assuming a shape for the curves, so I am not sure what the gamma distribution really brings here. In general, the use of a purely empirical approach may not be a problem in itself, but the authors should state that this is the approach taken and explain why.

Author Response: Using parametric distributions in statistics, such as the Gamma distribution, has many benefits, but the reviewer is correct that there is no extremely firm theoretical basis for such a statistical approach. The Gamma distribution has a wide range of applicability, and also covers the special case of an exponential distribution. Thus, we believe that this is a good starting point for readers who do not want to use lookup tables to provide a probability estimate for a given temperature drop measured anyware to compare a new measurement with the existing ones.

We however see the reviewer's point and suggest to use the empirical cumulative distribution estimates in Table 3. In our discussion version these values could be calculated from Eq. (2) with the parameters given in Table 2, and thus are somewhat redundant information. With the suggested changes we would have distribution-independent information in Table 3, which is certainly an improvement.

P35, Table 3: we now show the empirical probability distribution and rearranged the table to have the largest temperature drops on top of the table, and the weakest (actually increase in temperature) at the bottom.

Reviewer: The figures are generally of good quality but occasionally the captions should be edited so that the figures can be understood without reference to the main text.

Author Response: We will revise the captions accordingly.

P21, P22, P24: These figure captions were updated to make them stand-alone without reference to the text.

Reviewer: The caption to figure 2 was particularly obtuse from this point of view.

Author Response: Originally, the individual panels were separate figures with relatively long captions. With the aggregation to one figure with five panels, we had to reduce the caption length and thus information content. Obviousely we shortened the text too much and are happy to expand it in the revision to make this figure better understandable independently from the main text.

P21: Caption to Figure 2 was expanded accordingly.

Reviewer: In Figure 8 I didn't understand why and how the probability was used – shouldn't this be explained in the main text, if it is really needed at all.

Author Response: The basic principle of statistical comparisons is to compare a given result (i.e. our measurements) with a potentially fully random result. As mentioned in the caption we used the uniform distribution (i.e., each wind direction change is as likely in a random system) for comparison. If our measurements do not deviate from such a random outcome, the ΔProbability value is 0.00; if it is > 0, then our measurements indicate higher probability during solar eclipse than what we would expects in a random system (and if it is < 0, the probability is lower).

We will find a better way to describe this. We assume that using the term "probability" in the blue text items on the figure was confusing this reviewer. Of course one can always also debate on what a random outcome would be (we assumed uniform distribution), but we do not interpret this feedback in the way that this assumption was questioned.

P27: During the revisions we realized that using the term "Frequency" instead of "Probability" in this figure might have clarified some of the confusion. Hence we modified Figure 8 and its caption accordingly.

Reviewer: And on Figure 10, I (personally) think wind vectors would be a clearer way to indicate the change, which would then fit better with your figure 1. The use of colour to indicate flow directions is not intuitive.

Author Response: The key issue is the following: if a wind vector is presented, most readers confuse the angle of the vector with the geographic direction of wind (see example in Fig. 1 in our author response). It is almost impossible to present wind direction ***differences*** *in the same way as absolute wind directions are presented. That's why we used symbols with colors to represent the wind direction* ***differences*** *on these panels. In general the blue–red gradient is widely used in meteorology to show negative–positive deviations from something (e.g. temperature anomalies). What we could do is to simplify the color scheme to only use the blue–red gradient with white at zero difference instead of the rainbow-color-gradient currently used in Figure 10 to be more intuitive with our color scheme.*

Initially we of course hoped to find a way to subtract the local influence on wind direction from the measurement in a way that would leave us with the synoptic large-scale wind direction, but this proved almost impossible in the complex terrain of Switzerland; even the low-laying parts which are $\pm$flat actually experience channeled flow (as shown by Wanner and Furger, 1990, cited in our paper).

We showed an example in our author response. With respect to the color gradient a short investigation among colleagues suggested to keep the color gradient as is, since this is not uncommon. We suggest to keep the figure as is.

Reviewer: P1 L3-4 This sentence is confused between eclipse meteorology and the broader scientific benefits of studying eclipses.

Author Response: (actually on P2) We'll revise the text to eliminate this confusion and separate the two aspects more clearly.

P2/L6–7: Simply deleting this confusing sentence seems to be the best solution, hence we deleted it.

Reviewer: P1 L34 Should this be 1600km?

Author Response: (actually on P2) Yes, this was a typo, thank you for making us aware of it. Corrected.

P3/L8: corrected.

Reviewer: P2 L3-4 This sentence is ambiguous about whether a total or partial eclipse was seen at the two quoted locations. I believe the 1999 eclipse was total over south west England which would imply it was 97% at Reading and perhaps total at the other location, but please check and clarify.

Author Response: (actually on P3) We'll reword. See also our explanation of the confusion between partial and total eclipses below. A partial eclipse by definition is an eclipse that has no location on the Earth where totality can be seen. Thus, we need to be more clear about partial occultation during the event of a total eclipse vs. partial occultation of a partial eclipse. This will be reworded.

P3/L12: we now state that this was a total eclipse with maximum occultation of 97% at Reading. We also added Saros numbers to all eclipses mentioned in the text.

Reviewer: P4 L26 I am not sure what you mean by "model" - are you simply referring to the loess fitted values?

Author Response: Yes, this is the model fit. We will revise the wording to avoid potential misunderstandings. In statistics a "model" is everything fitted to the data which goes beyond the data themselves, but the term is not used in this way everywhere; e.g. "modelers" using global circulation models try to make the separation between "model" as the whole system and "modules" or "algorithms" for simpler statistical and prognostic model components. We will most likely refer to the "fit" in our revised version to avoid the confusion with the term "model".

P5/L6: we changed the text to read "…penumbral shading and these fitted values…"

Reviewer: P4 L28 is "instationarities" a proper word?

Author Response: The proper word is probably "non-stationarity" but we will double-check with an expert in both English and time-series statistics for the revisions.

P5/L8: after a careful investigation it turned out that the wording was correct, but that singular would be better suited. Hence we changed to "because of instationarity shortly before, …".

Reviewer: P5 I recommend moving most of the material on this page to the sections where you actually discuss each effect, as explained above.

Author Response: This refers to Sections 2.3 to 2.8 in the discussion version of our paper. The suggested reorganisation can of course be done. We will revise our manuscript accordingly.

Text was reorganized as suggested, see our response with detailed page/line numbers above.

Reviewer: P5 L18 Can you explain what this does so that people who don't use this particular software are able to reproduce your work?

Author Response: Yes, we will expand this text and provide an additional general reference to bootstrapping (which can be done in many ways, but maybe the term is not yet as widely known as we thought). In short, nonparametric bootstrapping is a computer-intensive method to obtain a best estimate for statistical uncertainty (e.g. the 95% confidence interval as we do it here) by performing many simulations with subsets of data records randomly selected out of all available records. In this way uncertainty related to individual outliers or extreme values in a given dataset are becoming less important for the uncertainty estimate, and thus the uncertainty estimate obtained via nonparametric bootstrapping is a rather robust and reliable uncertainty estimate. We will explain this in more detail in the revised version.

P8/L30–33: This text was added to explain the basics of bootstrapping uncertainty boundaries: "Bootstrapping is an efficient computer-based method to quantify uncertainty intervals (e.g. Efron, 1979; Johns, 1988). Nonparametric bootstrapping means that the uncertainty calculations are done on randomly selected subsets of all data points available in such a way that the variation in the results obtained from many repetitions (9,999 repetitions in our case) represents the uncertainty of the estimate."

Reviewer: P6 L4 Why gamma? (as discussed above)

Author Response: See response above with our suggestion for the revisions.

P9/L9–14: The Gamma distribution has a wide range of applicability, and also covers the special case of an exponential distribution. Thus, we believe that this is a good starting point for readers who do not want to use lookup tables to provide a probability estimate for a given temperature drop measured anyware to compare a new measurement with the existing ones.

We however see the reviewer's point and thus now present the empirical cumulative distribution estimates in Table 3.

Reviewer: P6 L7 Both SE and SD are used for errors in this paper, can you be more consistent?

Author Response: The meaning of SE and SD is not the same, hence we use either or depending on what the context is: SE is the standard error of the mean and describes the uncertainty of the mean. SD is the standard deviation and describes how far a way from the mean a single observation lies. To obtain SE for the mean of a time series we would have to correct for serial autocorrelation, which is another confusion that many readers (even those with adequate statistical background) normally have, and hence we avoided to go into this aspect of serial autocorrelation by simply using the purely descriptive SD (e.g. for difference in short-wave radiation).

We can of course modify our text and consistently report SE also for the time series.

P7/L3: we now give mean $\pm$ SE for the short-wave radiation here.

Reviewer: P7 eq 4. Is this another example of an entirely empirical fit, or is there some reason why the diffuse fraction varies with time during the day that is not explained?

Author Response: Yes, this is an empirical fit. Unfortunately, the sky was not perfectly cloudless during the eclipse. That the ratio between diffuse and direct radiation is a function of solar elevation angle is well known, but we should have explained this in the text. Here we used Δt (time difference from local noon) for simplicitly, but we probably should better first calculate the solar elevation angle and then use this as the independent variable instead in order to be more physically-based. The parameter estimates would still be empirical best fits, but with elevation angle instead of Δt as the independent estimate.

P7/L23–24: We tried out options to use solar elevation angle instead of Δt, but results were poorer and thus we left the empirical fit as it was, but added the text "This empirical fit was used because α was not a simple function of the solar elevation angle (fit not shown)."

Reviewer: P7 L7 Explain image analysis here rather than in the methods

Author Response: This will be done.

P7/L28–32: done.

Reviewer: P7 L17-20 Are you effectively working out the long wave albedo here? And if so, would it help to say that?

Author Response: According to Glickman, T. S. (ed.) (2000), Glossary of Meteorology, American Meteorological Society, http://glossary.ametsoc.org/wiki/Albedo the definition of albedo is: "Albedos commonly tend to be broadband ratios, usually referring either to the entire spectrum of solar radiation, or just to the visible portion." This does not include long-wave radiation and thus we do not think that a ratio between back-radiated long-wave radiation (which is a fraction of the long-wave radiation emitted by the Earth surface, not a radiation component from the sun) and emitted long-wave radiation should not be termed "albedo". We however realized that the term is used in some papers and textbook, hence we suggest to write about long-wave radiation balance and add the term "long-wave albedo" with quotes and in parentheses.

P8/L2: we struggled with the term "longwave albedo" but since it seems to appear in some texts, we added it in parentheses with quotes in the hope that this clarifies our text.

Reviewer: P7 L31 explain bootstrapping here rather than in methods section

Author Response: This will be done.

P8/L26–33: done.

Reviewer: P8 L4 would it help to compare the temperature changes in the literature for partial versus total eclipses, even if it is just to show there is no real difference?

Author Response: This comment is fully understandable and we initially also struggled with terminology. The astronomical terminology uses the terms "total", "partial" and "annular" eclipses. With all three there can be "partial occultation" (as we call it), but in the case of a partial eclipse there is no location on the earth with totality. The theoretical differences in solar short-wave radiation remaining is small between total and annular eclipses, and partial occultation of a given fraction at a site should not depend on the fact whether an eclipse is partial or total. In our understanding much of the temperature drops reported in the literature are strongly affected by cloudiness during the time of observation. This means that if we were to dwell more into analysing various factors we would have to separate the effects of total vs. annular (only very few reports) vs. partial eclipses as a function of degree of occultation and cloudiness. Information on cloudiness is however in most cases not a quantitative information that could be easily used for such an investigation and hence we decided not to add such an analysis.

As explained in detail in our author response, we decided not to further separate the dataset in the suggested subsets.

Reviewer: P8 L6-8 See comments above

Author Response: We will move the information from Section 2.8 here and show empirical cumulative distribution estimates in Table 3 instead.

P9/L9–14: done. We deleted the information about the mean and standard error of the Gamma distribution since it was not relevant for our study and may have added to some confusion before.

Reviewer: P8 L15 Can you take a couple of sentences to explain the normal diurnal variation in the mountain valley winds? This seems a unique local meteorology that not everyone will be familiar with.

Author Response: Yes, will will do this. Most likely other readers will also benefit from a short introduction on mountain valley wind systems.

P9/L29–33: we added the following text: "A mountain valley wind system is characterized by down-valley winds at night that contrast with up-valley winds during the day when solar irradiation on the mountain slopes leads to convective uplifting of air masses, thereby leading to up-slope and up-valley winds. At night, the radiative cooling on the same valley slopes leads to the production of cold air, which is denser than the surrounding air, and hence moves down-slope and down-valley (also known as katabatic drainage flow)."

Reviewer: P11 L18 Annular eclipses don't cause full occultation, and in terms of the meteorological effects are analogous to partial rather than total eclipses.

Author Response: We will reword. We did not claim that the effects were the same, but we wanted to express that most literature reports on temperature drops are either from total eclipses, or from annular eclipses, whereas reports on temperature drops from partial eclipses are rare. We'll carefully revise to avoid potential confusion in our statement.

P18/L9: we exchanged the word "full" by "maximum" to clarify: "…most temperature drop reports in the literature relate to maximum occultation during total and annular eclipses."

Reviewer 2

Reviewer: This work provides a thorough analysis of eclipse-induced responses as observed by a Swiss network of meteorological sites. A complexity of this region is of course the range of topogaphy encountered, and the authors carefully separate the data obtained in different conditions. These reveal the wind direction and thermal changes, which are compared with previous studies. This is a valuable contribution to the literature and should be published.

In addition, the measurements in Switzerland are uniquely position to investigate the original interpretative ideas of Clayton, modified a century later by Aplin&Harrison. The scales employed are appropriate for this as they consider a large part of the European landmass away from coastal effects. Proper consideration of the remaining topographical aspects, as undertaken by the authors is therefore important in obtaining the underlying effects on the dynamical structures arising from eclipse meteorology.

Author Response: Thank you very much for this positive assessment.

Reviewer: Minor points p1 L7 sun's disk

Author Response: This will be corrected.

We changed this throughout the manuscript (e.g.: P2/L10, 13, 14).

Reviewer: p1 L14 comma after "After the maximum,.."

Author Response: This will be corrected.

P2/L18: done.

Reviewer: p1 L27 it's – > its

Author Response: This will be corrected.

P2/L32: done.

Reviewer: p9 L24 for

Author Response: This will be corrected.

P11/L8: done.

Reviewer: p10 L1 mountain

Author Response: This will be corrected.

P12/L27: done.

Reviewer: fig1 last line "its"

Author Response: This will be corrected.

P20, line 4 in figure caption shows the correction.

Reviewer: Section 2.6 Give some explanation of the consequences for the choice of the sill and range parameters

Author Response: This can be done. In fact, the sill and range parameters do not strongly affect the interpolation and the main differences between choices that we tested out were affecting the borders of the range covered with data. As an example we included the variants for all data with sill/range of 90°/10 km, 120°/10000 km, and 300°/1000 km. Thus, the initial estimates for both parameters are not essential and the model fit nicely finds the best estimate. This is the ideal case if no attractors exist within the realistic domain of search of the optimization algorithm.

P11/L12–16: we added the following text: "We tested the range 90°–300° for the partial sill setting, and 10–10,000 km for the range setting. The results were similar due to the optimization method used in Kriging and differed only in very minor details (see examples in our response, doi:10.5194/acp-2017-321-AC2). The selection for the final computations was thus based only on the facts that a 300° (or –60°) corresponded to the typical deviation angle of wind directions under cyclonic influence, and that 1000 km covered the entire domain of Switzerland."

Additional Edits

P1, Title: Temperature and wind direction are now in singular in the title

P1/L17–P2/L3, Abstract: Contents rearranged to better emphasize the main findings

P3/L27–34: Slightly reworded the text

P11/L8–9: We added a sentence on the low level jet over the Swiss Plateau (in relation to what Gray and Harrison 2016 considered a new valid interpretation of the wind direction changes observed in the UK).

Effects of vernal equinox solar eclipse on ~~temperatures~~temperature and wind ~~directions~~ direction in Switzerland

Werner Eugster[1], Carmen Emmel[1], Sebastian Wolf[2], Nina Buchmann[1], Joseph P. McFadden[3], and C. David Whiteman[4]

[1]ETH Zurich, Department of Environmental Systems Science, Institute of Agricultural Sciences, 8092 Zurich, Switzerland
[2]ETH Zurich, Department of Environmental Systems Science, Institute of Terrestrial Ecosystems, 8092 Zurich, Switzerland
[3]University of California, Santa Barbara, Department of Geography, Earth Research Institute, Santa Barbara, California, 93106–4060, USA
[4]University of Utah, Atmospheric Sciences Department, Salt Lake City, Utah, USA

Correspondence to: W. Eugster (eugsterw@ethz.ch)

Abstract. The vernal equinox total solar eclipse of 20 March 2015 produced a maximum occultation of 65.8 to 70.1% over Switzerland during the morning hours (09:22 to 11:48 CET). Skies were generally clear over the Swiss Alps due to a persistent high-pressure band between the UK and Russia associated with a rather weak pressure gradient over the continent. To assess the effects of penumbral shading on near-surface meteorology across Switzerland, air temperature data measured at 10-minute intervals at 184 MeteoSwiss weather stations that reported air temperature at 10-minute intervals were used. Wind speed and direction data were available from 165 of these stations. Additionally, six Swiss FluxNet eddy covariance flux (ECF) sites provided turbulent measurements at 20 Hz resolution.

During maximum occultation the temperature drop was up to 5.8 K at a mountain site where cold air can pool in ~~the topographic depressionof the weather station~~a topographic depression. The bootstrapped average of the maximum temperature drops of all 184 MeteoSwiss sites during the solar eclipse was 1.51 ± 0.02 K (mean $\pm$ SE). A detailed comparison with literature values since 1834 showed a temperature decrease by 2.6 ± 1.7 K (average of all reports), with extreme values up to 11 K. On fair weather days under weak larger scale pressure gradients, local thermo-topographic wind systems develop that are driven by small-scale pressure and temperature gradients. At one ECF site, the penumbral shading delayed the morning transition from down-valley to up-valley wind conditions~~, and at~~. At another site, it prevented this transition from occurring at all. Data from the 165 MeteoSwiss sites measuring wind direction did not show a consistent pattern of wind direction response to the passing of the penumbral shadow. These results suggest that the local topographic setting had an important influence on the temperature drop and the wind flow patterns during the eclipse. ~~Still, results tend to lend support to a recent theory that the anticyclonic cold-air outflow from the center of the eclipse only extends~~ A significant cyclonic effect of the passing penumbral shadow was found in the elevation range ~~≈1600 km outwards, with cyclonic flow beyond that distance~~1700–2700 m a.s.l., but not at lower elevations of the Swiss Plateau. This contrasts with an earlier theory that the anticyclonic outflow should reach as far as ≈2400 km from the center of the eclipse, which would have included all of Switzerland during the 2015 eclipse. ~~Nevertheless, a significant cyclonic effect of the passing penumbral shadow was found in the elevation range ≈1700–2700 m a.s.l., but not at lower elevations of the Swiss Plateau.~~ Thus, measurable effects of penumbral shading on the local wind system

could be even found at ≈2000 km from the path of the eclipse (that is, Switzerland during the 2015 eclipse), and our results tend to lend support to a newer theory that the anticyclonic cold-air outflow from the center of the eclipse only extends ≈1600 km outwards, with cyclonic flow beyond that distance.

1 Introduction

Solar eclipses have long fascinated scientists and brought about essential scientific knowledge on the meteorologial effects of the phenomenon. ~~This has led to major discoveries such as the existence of helium or the high temperature of the corona (Pasachoff, 2009), but the~~ The most commonly studied effect is that on temperature at Earth's surface (Table 1, Aplin et al., 2016). Less, however, is known about the effects on local and larger scale wind directions at places where only partial occultation is observed. Here we test the hypothesis that even a partial occultation of a solar eclipse may have short-term influences on wind directions. During a solar eclipse, the new moon passes in front of the sun's disk and thus reduces incoming solar radiation. This astronomic event is typically described with four phases. It begins with the first contact between the moon and the sun as seen by an observer on the Earth. With the first contact, the penumbral shading begins, that is the partial shading where ~~sunrays~~ sun rays from one part of the sun's disk are blocked by the moon~~whereas sunrays~~, whereas sun rays from the opposite side of the sun's disk still reach the observer. This phase ends with the second contact when the moon completely obscures the sun and the observer is in the dark shadow of the moon. During this second phase of totality, only diffuse sunlight reaches ~~the~~ Earth's surface. This phase ends with the maximum occultation, when the solar corona can be seen in the ~~special~~ case of a total eclipse. With annular and partial eclipses, the maximum occultation simply means the darkest conditions. After the maximum, light levels increase again until the third contact, when the transition from the umbral shadow to the less dark penumbral shadow takes place. The ~~astronomic~~ astronomical event ends with the fourth contact, after which meteorological conditions should no longer depend on the moon's position. The second and third contacts are ~~only observed~~ observed only in the narrow band of the umbra during annular or total eclipses.

During the total vernal equinox eclipse of 20 March 2015 ~~,~~(Saros 120, https://eclipse.gsfc.nasa.gov/5MCSE/5MCSE-Maps-10.pdf), which produced a partial occultation over the Swiss Alps, the weather conditions were excellent with mostly clear skies due to a persistent high-pressure band between the UK and Russia, with a rather weak pressure gradient over the continent (MeteoSwiss, 2015). On normal days under weak larger scale pressure gradients, local thermo-topographic wind systems develop that are driven by small-scale pressure and temperature gradients, which are strongest in mountainous areas such as the Swiss Alps. It could hence be expected that during penumbral shading, these thermo-topographic winds would be subject to modifications superimposed by the larger scale circulation generated around the umbra of the solar eclipse. The meteorological conditions during an eclipse are expected to be the same as that of a "cyclone with a cold centre" as described by Ferrel (1890, pp. 337–342). In such a cyclone, the vertical motion is reversed as compared to a typical warm centered cyclone. This leads to a (narrow) core with cyclonic rotation in the cold center of the cyclone and an anticyclonic counterflow around this core. Because of ~~it's~~ its reversed structure, the cyclonic rotation in a cold-centered cyclone according to Ferrel (1890) is strongest in

the upper troposphere and weakest near the surface, whereas the anticyclonic rotation is weakest in the upper troposphere and strongest near ~~the~~ Earth's surface.

Based on Ferrel's (1890) concept, Clayton (1901) empirically determined the direct influence of the occultation on wind direction within the shaded area during the 28 May 1900 total eclipse (Saros 126). According to Clayton's (1901) theory, the cyclonic rotation in the center of the umbra is not detectable, but an anticyclonic outflow should be generated in the inner zone of the penumbral shadow. This zone with anticyclonic rotation is expected to extend at least 2400–3200 km (1500 to 2000 miles; Clayton, 1901) from the center of the umbra. In contrast, the outer part of the penumbra is subject to a cyclonic wind direction rotation (a further ≈1600~~m~~ km; Fig. 1a). Although Clayton (1901) ~~concludes~~ concluded that this rotational pattern "confirms so well Ferrel's theory of the cold-air cyclone", he ~~does~~ did not provide an estimate of the dimension or strength of the cold-air cyclone in the center of the umbra because no cyclonic effects could be seen in his analyses. Following Clayton (1901), Aplin and Harrison (2003) carefully assessed the penumbral winds at Reading and Camborne (UK) during the 11 August 1999 ~~eclipse where~~ total eclipse (Saros 145) of which a maximum occultation of 97% was observed at Reading. Their 1 Hz ultrasonic anemometer wind speed and wind direction measurements showed a pronounced drop in wind speed during the eclipse. The wind then changed in a cyclonic ~~way~~ direction on first contact, and later returned via an anticyclonic rotation to the synoptic wind direction after maximum occultation. Thus, their finding conformed to what is expected for the inner core around the umbra, where Clayton (1901) expected the cold-air cyclone, but did not find it in his own analysis of synoptic-scale weather maps. Aplin and Harrison (2003) thus postulated a revised model with an inner cold core of ca. 160 km around the center of the umbra containing cyclonic flow (Fig. 1b). They expected an anticyclonic rotation outside this zone that extends to ca. 1600 km (1000 mi), with a further outermost zone of cyclonic rotation then extending up to ca. 4800 km (3000 mi).

Bilham (1921) was the first to empirically confirm an indirect effect of the cooling during occultation on wind direction. He ~~reports~~ reported that "the wind showed a marked tendency to back" (as expected from cyclonic influence of the thermal wind), consistent with the cold-core cyclone in the umbral zone. There is observational evidence of thermal wind effects superimposed on near-surface winds during occultation, but no regional-scale weather prediction model has been able to reproduce this effect successfully. Prenosil (2000) simulated the 11 August 1999 eclipse in Central Europe using a hydrostatic regional weather prediction model. This model was able to produce a slight cyclonic circulation in the surface winds, but it only lasted for some minutes and thus challenges the idea that such a weak effect can be observed in field measurements.

~~For the Swiss Alps during the~~ During the vernal equinox eclipse of 2015, ~~there is~~ we expected a clear difference in ~~expected wind direction between the Clayton (1901) and~~ wind direction for the Swiss Alps dependent on the Clayton (1901) or the Aplin and Harrison (2003) theories~~that motivated the authors to investigate~~ . Thus, we investigated whether the onset of penumbral shading leads to an anticyclonic (following Clayton's theory; Fig. 1a) or a cyclonic (following Aplin and Harrison's theory; Fig. 1b) influence on near-surface wind directions. We hypothesized that during maximum occultation (66–70% across Switzerland, ≈2000 km away from the umbral center), ~~the influence should be anticyclonic according to Clayton (1901) (Fig. 1a) or cyclonic according to Aplin and Harrison (2003) (Fig. 1b).~~ Switzerland was in the ideal position to determine which of the two theories is closer to reality. Our aim in this paper is thus to extend the analysis of temperature drops during occultation to assess whether

available wind direction data can support one of the two theories about air mass circulation inside the penumbra during the eclipse.

2 Material and Methods

The vernal equinox eclipse of 20 March 2015 was a Saros 120 total eclipse (partial in Switzerland), with its maximum at 09:45:39 UTC (10:45:39 CET; NASA, 2015). In Switzerland, occultation started with the first contact of the sun and moon disks at 09:21:58 CET in Geneva (western border) and ended with the fourth contact at 11:47:49 CET in Martina (eastern border). Maximum occultation ranged from 65.8% in Chiasso (southern border) to 70.1% in Bargen/Schaffhausen (northern border). The timing of maximum occultation varied from 10:29:26 to 10:35:55 CET across Switzerland (NASA, 2017). The second and third contact of a total eclipse are the entering ~~to~~ into and exiting from the umbra, respectively. In areas with only partial occulation, the second and third contact do not occur.

This eclipse has been thoroughly investigated with a focus on the mainland UK in a themed issue with 16 papers introduced by Harrison and Hanna (2016). Although all contributions are relevant, we specifically refer only to the articles with a direct link to our own study (Aplin et al., 2016; Clark, 2016; Good, 2016; Hanna et al., 2016; Burt, 2016; Pasachoff et al., 2016; Gray and Harrison, 2016; Portas et al., 2016; Barnard et al., 2016).

2.1 Sites and data

We used six Swiss FluxNet sites (www.swissfluxnet.ch; Table S1) with 20 Hz ultrasonic anemometer–thermometer data and 184 conventional MeteoSwiss weather stations (Table S2) across Switzerland and Liechtenstein (MeteoSwiss, 2017), of which 165 ~~also supplemented the temperature data with~~ not only provided temperature data but also wind speed and wind direction measurements (Table S3). We used data from 20 March 2015 and—where possible—the previous one or two days for reference. All three days were nearly clear, except for occasional scattered high-level clouds.

Sensors used at the MeteoSwiss station are Pt-100 thermistors for temperature measurements and Lamprecht L14512 cup anemometers with a wind vane for wind speed and wind direction measurements. Some sites alternatively use 2-D ultrasonic anemometers (MeteoSwiss, 2017). At the Swiss FluxNet sites, the specific instruments included in this study ~~are~~ were Gill HS or R3 ultrasonic anemometers (Gill Ltd., Lymington, UK), Kipp and Zonen CNR-1 four-way net-radiometers (Delft, the Netherlands) with active ventilation (Markasub, Olten, Switzerland). Only at the CH-OE2 site, a Delta-T BF5 sunshine sensor (Cambridge, UK) was available for measurements of diffuse and total photosynthetic photon flux density (PPFD). PPFD is the quantum flux in the visible range 400–700 nm that plants use for photosynthesis.

For all these variables except temperature (see Section 2.2) and wind direction (see Section 3.4), the difference between 20 March and either 18 or 19 March was calculated, depending on which of the two previous days had closer to clear-sky conditions. ~~For temperature comparisons we~~ We used two different concepts to determine the drop in temperature (see Section 2.2).

2.2 Calculation of temperature drop

All analyses were done with R version 3.3.1 (R Core Team, 2016). The local temperature effect at each site was estimated by fitting a local polynomial regression with a span parameter of 0.1 ("loess", a locally weighted least squares regression function in R) to each time series from 20 March~~, for which the~~ . The measurements during the penumbral shading and the adjacent 12 minutes on both sides were excluded from the fit. The maximum difference between the measurements during penumbral shading and these ~~model~~ fitted values was then determined. This approach closely ~~follows~~ followed the method used by Segal et al. (1996), or the linear approach used by Clark (2016). In a few cases (sites GRH, ROG, ULR, VAD, VSBLI; see Table S2), however, this approach failed (e.g. because of ~~instationarities~~ instationarity shortly before, shortly after, or during the time period of the eclipse, which can lead to erratic interpolations) and thus the simple temperature difference with respect to 19 March ~~had to be~~ was used. We did not use this latter approach for all sites because there were substantial temperature differences between 18, 19 and 20 March 2015, despite persistent and very similar fair-weather conditions. The period of interest coincided with the peak spring snowmelt. For example, at the CH-FRU mountain grassland flux site (1000 m a.s.l.) where four phenological camera images were taken per day, the snow cover in the morning of 18 March 09:30 CET was still around 80%, but declined strongly during 18/19 March and had less than 10% coverage by the evening of 19 March at 18:30 CET. On 20 March, the site was basically free of snow, similar to other mountainous stations that were subject to snowmelt.

2.3 ~~Calculation of long-wave radiation effect~~

~~To quantify the eclipse effect on long-wave back-radiation from the sky we determined the difference between the two long-wave flux components from 20 March 2015 and the reference day before,~~

$$\Delta LW_x = LW_x(\text{20 March}) - LW_x(\text{19 March}) \,,$$

~~where x is the incoming (in) or the outgoing (out) long-wave radiation component. Then, two linear regressions between ΔLW_{in} and ΔLW_{out} were calculated with the 1-minute averages of the CH-OE2 site, (a) for the period of the eclipse (09:26–11:42 CET), and (b) for the times of day not including the period of the eclipse.~~

2.3 ~~Calculation of wind direction effect~~

~~The effect of penumbral shading on wind direction was determined by comparing (a) a 1-hour reference period that ended 12 minutes before the first contact with (b) the first half of penumbral shading (from first contact to maximum occultation, which was roughly 1.1 hour). For both periods, the vector-averaged mean wind direction was computed, and then the rotation angle was determined. The same procedure was repeated for the same time periods of 19 March, and the difference in rotation angle was calculated as the net effect of penumbral shading used in this study.~~

2.3 ~~Bootstrapping of uncertainty bounds~~

To quantify the uncertainty of the temperature drop and wind direction effects as a function of elevation, we employed nonparametric bootstrapping with the "boot" or Bootstrap Resampling package of R in combination with the "loess" function with a span of 0.5 to describe the temperature drop or wind direction effect as a function of elevation. Elevations were binned in 10-m intervals for the bootstrap procedure, which was repeated 9,999 times. 95% statistical confidence intervals were then determined from the output.

2.3 Spatial interpolations

Wind direction effects were spatially interpolated with ordinary Kriging using the krige.conv function of the geoR package of R. The partial sill parameter was set to 300°, and the range parameter was set to 1000 km.

2.3 Image analysis

The potential effect of cloudiness during the eclipse was investigated by analyzing a sequence of phenological camera images recorded every two minutes during the eclipse (4× per day otherwise) for the brightness of the vegetation. For this, we used the ImageJ software as implemented in the Fiji image processing package, version 2.0.0 (http://imagej.net/Fiji). The vegetation brightness is simply the normalized gray value of the image region that was manually defined as "vegetation". A brightness of 100% corresponds to a white image, and 0% is black.

2.3 Gamma probability distribution fit

We fit a Gamma probability density function to the histogram of the maximum cooling ΔT during the eclipse,

$$f(\Delta T) = \frac{1}{s^a \cdot \Gamma(a)} \cdot (\Delta T - T_0)^{a-1} \cdot e^{\frac{T_0 - \Delta T}{s}} ,$$

where ΔT is the maximum temperature drop during an eclipse event (a positive value), and a and s are the shape and scale parameters of the probability density function $f(\Delta T)$, respectively. Γ is the Gamma function, and T_0 is the reference value (or offset) of ΔT to fit the peak of the probability density function $f(\Delta T)$ to the data. The mean of the distribution $f(\Delta T)$ is $a \cdot s$, and its standard error is $\sqrt{a \cdot s^2}$.

3 Results and Discussion

3.1 Short-wave radiation effects

Incoming short-wave radiation can be used as a control for correct timing and magnitude of the occultation. Standard MeteoSwiss weather stations, however, only record 10-minute averages, which are too coarse for an in-depth assessment. The Swiss FluxNet sites use averaging times ranging from 10 to 30 minutes (Table S1), with the exception of the CH-OE2 cropland and CH-DAV forest sites where 1-minute averages of all four radiation components were available. Diffuse and total PPFD

were also measured with the same resolution at CH-OE2, and thus we used data from CH-OE2 as an example here. The expected reduction of incoming short-wave radiation was ≈70% (Fig. 2a) during maximum occultation of the sun's disk (≈70%). The difference between measured and expected incoming short-wave radiation ~~is~~ was –9.8 ± ~~2.4~~ 0.7 W m^{-2} (mean ± ~~SD~~SE). For a second class pyranometer such as the CM3 model used in the CNR-1 radiometer, this is the order of magnitude of the accuracy. However, the timing of the radiation minimum in Figure 2a was not exactly as expected assuming that minimum radiation should be observed at the time of maximum occultation: the theoretical radiation level during maximum occultation was reached 19 minutes before the eclipse's maximum. Most likely, this was a confounding effect due to minor high-level Cirrostratus clouds passing at that time~~. The~~ ; the fraction of diffuse radiation already started to increase shortly after the first contact on 20 March (Fig. 2b), whereas on the previous day, a curvilinear decrease was observed as expected during this early morning period with rising solar elevation. Cirrostratus clouds are the likely cause since images taken every two minutes during the occultation phase at the site do not indicate any signs of medium and low-level clouds. This coincidence of shading by cirrostratus clouds and occultation of the sun may have led to the stronger than expected decrease in short-wave radiation levels and the earlier than expected radiation minimum.

To test this hypothesis, we made an attempt to empirically correct measured short-wave incoming radiation for potential concurrent cloud shading that leaves a trace in the fraction of diffuse radiation (Fig. 2c). The assumption we ~~make~~ made for such a correction ~~is~~ was that no change in the ratio of diffuse vs. direct radiation would occur due to the occultation of the sun's disk alone. Thus, if we assume that the diffuse radiation (expressed as absolute radiation flux density) remains unaffected by the cirrostratus clouds, then we can correct this effect with

$$SW_{in,\,corr} = \frac{\alpha}{\alpha_{fit}} \cdot SW_{in}\ , \tag{1}$$

where SW_{in} and $SW_{in,\,corr}$ are measured and corrected incoming short-wave radiation, and α and α_{fit} are ratios of diffuse and direct radiation for the measurements and the model, where the empirical best fit for α_{fit} used in the model (Fig. 2c) is

$$\alpha_{fit} = \frac{\textit{diffuse radiation}}{\textit{direct radiation}} = (0.674 \pm 0.002) + (0.0452 \pm 0.0002) \cdot (\Delta t)^2\ , \tag{2}$$

with Δt being the time difference to local noon (12:36:45 CET on 20 March 2015) in hours. This empirical fit was used because α was not a simple function of the solar elevation angle (fit not shown). The resulting $SW_{in,\,corr}$ (red line in Fig. 2a) still ~~does~~ did not show a symmetric effect before and after the short-wave radiation minimum. An analysis of images during that period (Fig. 2d) also ~~indicates~~ indicated that the shading effect was not symmetric during occultation: the image brightness decreased very quickly after first contact, but then remained almost constant, irrespective of the fraction of occultation of the sun~~disk. Both observations indicate~~ 's disk. This potential effect of cloudiness during the eclipse was investigated by analyzing the brightness of the vegetation in a sequence of phenological camera images that were recorded every two minutes during the eclipse (4× per day otherwise). For this, we used the ImageJ software as implemented in the Fiji image processing package, version 2.0.0 (http://imagej.net/Fiji). The vegetation brightness is simply the normalized gray value of the image region that was manually defined as "vegetation". A brightness of 100% corresponds to a white image, and 0% is black.

Both observations—diffuse/direct radiation measurements and camera images—indicated a confounding effect of cirrostratus cloud passage.

3.2 Long-wave radiation effects

To quantify the eclipse effect on long-wave back-radiation from the sky (sometimes referred to as "longwave albedo") we determined the difference between the two long-wave flux components from 20 March 2015 and the reference day before,

$$\Delta LW_x = LW_x(\text{20 March}) - LW_x(\text{19 March}) \,, \tag{3}$$

where x is the incoming (in) or the outgoing (out) long-wave radiation component. Then, two linear regressions between ΔLW_{in} and ΔLW_{out} were calculated with the 1-minute averages of the CH-OE2 site, (a) for the period of the eclipse (09:26–11:42 CET), and (b) for the times of day not including the period of the eclipse.

The reduction in short-wave radiation also ~~reduces~~ reduced energy dissipation at Earth's surface, which in turn ~~reduces~~ reduced long-wave emitted radiation (LW_{out}, Fig. 2e, blue line). The reduction in LW_{out} ~~is~~ was symmetric during the penumbral shadow passage, supporting our interpretation that if a cloud passage confounded the SW_{in} term, then it most likely was a cloud type that ~~affects~~ affected short-wave radiation more than the long-wave radiation components. Cirrostratus may have this quality. However, the role of high clouds on ~~the~~ Earth's radiation budget is difficult to quantify (Boucher et al., 2013).

The reduction in LW_{out} ~~reduces~~ reduced the re-emitted sky radiation LW_{in} (Fig. 2e, black line). The regression between ΔLW_{in} and ΔLW_{out} (Fig. 3), i.e., the differences between the respective radiation component measured on the day of the eclipse and the day before the eclipse, ~~shows~~ showed an order of magnitude difference between the penumbral shading ($\Delta LW_{in} \approx 0.24$ ΔLW_{out}) and the unshaded conditions ($\Delta LW_{in} \approx 2.84$ ΔLW_{out}).

3.3 Direct effects on air temperature

Although radiation effects could ~~only~~ be investigated at only the two sites having 1-minute measurements, similar conditions were observed in 10-min data at all radiation measurement sites. All sites showed a reduction in 2-m air temperatures (Table S2). The strongest effect of –5.8 K was seen at an Alpine site (Fig. 4; VSSOR in Table S2) at 1987 m a.s.l. which was still completely snow covered during the eclipse. The topographic setting (Fig. 4) is a small basin surrounded by a larger catchment area of 7.5 km^2. The most important effect thus ~~appears~~ appeared to be the position of the weather station. It ~~is~~ was located in a closed topographical basin ca. 66 m below the mountain ridge. A cold-air pool building up during the eclipse could be drained towards the Rhone valley over this ridge. Had we taken the difference between 19 and 20 March for estimating the temperature effect, then this site would have yielded a difference of –8.8 K.

To quantify the uncertainty of the temperature drop (and wind direction effects) as a function of elevation, we employed nonparametric bootstrapping with the Bootstrap Resampling package of R in combination with the "loess" function with a span of 0.5 to describe the temperature drop or wind direction effect as a function of elevation. Elevations were binned in 10-m intervals for the bootstrap procedure, which was repeated 9,999 times. Statistical confidence intervals were then determined from the output at the 95% level. Bootstrapping is an efficient computer-based method to quantify uncertainty intervals (e.g. Efron, 1979; Johns, 1988). Nonparametric bootstrapping means that the uncertainty calculations are done on randomly selected subsets of all data points available in such a way that the variation in the results obtained from many repetitions (9,999 repetitions in our case) represents the uncertainty of the estimate.

The mean effect over the entire elevation range covered by MeteoSwiss weather stations (Table S2) as determined by non-parametric bootstrapping ~~is~~ was a reduction of 1.51 ± 0.02 K (mean $\pm$ SE; see Fig. 5). The weakest effects were found at the lowest elevation sites (<350 m a.s.l., reduction of 0.62 ± 0.06 K), and the highest elevation sites, where data coverage ~~is~~ was poor (>3150 m a.s.l., reduction of 0.69 ± 0.03 K).

Although the 20 March 2015 eclipse featured a partial occultation of 66–70% throughout Switzerland, the temperature effects (Fig. 5, Table S2) ~~are~~ were comparable to temperature reductions previously reported in the literature for all eclipse types (Fig. 6 and Table 1). We found no clear dependence of temperature reductions on eclipse type, geographic location ~~and~~ or other factors in the literature reports. Therefore, we summarized the data set by fitting a Gamma probability distribution to the data as shown in Figure 6. ~~This distribution~~ The Gamma probability density function

$$f(\Delta T) = \frac{1}{s^a \cdot \Gamma(a)} \cdot (\Delta T - T_0)^{a-1} \cdot e^{\frac{T_0 - \Delta T}{s}} \quad (4)$$

was fit to the histogram of the maximum cooling ΔT during the eclipse, where ΔT is the maximum temperature drop during an eclipse event (a positive value), and a and s are the shape and scale parameters of the probability density function $f(\Delta T)$, respectively. Γ is the Gamma function, and T_0 is the reference value (or offset) of ΔT to fit the peak of the probability density function $f(\Delta T)$ to the data. The distribution developed in this study will allow researchers to quickly assess ~~how likely it will be to find reports in the literature~~ the probability that the existing literature contains values that exceed a given measured temperature drop during an eclipse. The parameter estimates for the probability distribution (Eq. 4) are given in Table 2. The average temperature drop reported in the literature ~~so~~ thus far was 2.6 ± 1.7 K (based on Eq. 4, Table 2), while the mean drop calculated for our study was 1.5 ± 1.0 K. ~~Temperature~~ Already temperature effects of this (smaller) magnitude during occultation have the potential to induce thermal winds.

3.4 Wind direction effects

The effect of penumbral shading on wind direction was determined by comparing (a) the 1-hour reference period that ended 12 minutes before the first contact with (b) the first half of penumbral shading (from first contact to maximum occultation, which was roughly 1.1 hour). For both periods, the vector-averaged mean wind direction was computed, and then the rotation angle was determined. The same procedure was repeated for the same time periods of 19 March, and the difference in rotation angle was calculated as the net effect of penumbral shading used in this study.

The most striking effect on wind direction was found at two Swiss FluxNet sites with high-resolution 3-D wind velocity measurements. The timing of the solar eclipse between 09:22 and 11:48 CET across Switzerland (see Section 2) ~~coincides~~ coincided with the hours when the mountain valley wind system ~~changes wind~~ typically changes direction by 180° under normal conditions. ~~At the~~ A mountain valley wind system is characterized by down-valley winds at night that contrast with up-valley winds during the day when solar irradiation on the mountain slopes leads to convective uplifting of air masses, thereby leading to up-slope and up-valley winds. At night, the radiative cooling on the same valley slopes leads to the production of cold air, which is denser than the surrounding air, and hence moves down-slope and down-valley (also known as katabatic drainage flow). At the CH-DAV subalpine forest site (1639 m a.s.l.), the penumbral shading resulted in a delay of the onset of the daytime

wind direction by roughly one hour (Fig. 7), whereas at the CH-AWS alpine grassland site (1978 m a.s.l.) the shading even prevented the establishment of the diurnal up-valley wind altogether (Fig. 7). From 09:26:32 CET (first contact) to 11:46:37 CET (last contact), the short-wave radiation decreased by up to 68% (–447 W m^{-2}; 10-minute average) with respect to perfect clear-sky conditions two days before (18 March 2015). This delayed the down-valley to up-valley wind direction transition that was very had been pronounced on both preceding days. Further, the penumbral shading hindered the onset of up-valley winds in such a way that the down-valley winds persisted even after the ending of the shading shading had ended. This means that the valley wind blew in the opposite direction to what we would have predicted for comparable conditions without penumbral shading. The lack of reversal of wind direction might be could have been an effect of the cyclonic rotation in the outer circle of the penumbra as predicted by Aplin and Harrison (2003) for this distance of ≈2000 km from the umbra. This lack of reversal of wind direction at CH-AWS also occurred at a conventional agrometeorological weather station Michna et al. (2013) ca. 1 km further up-valley Michna et al. (2013).

Although the cyclonic effect appears appeared to be rather pronounced at CH-DAV and even more so at CH-AWS, most conventional weather stations do did not show a clear signal (Figs S1–S4). In principle, only sites located on a valley bottom (Fig. S2) are expected to respond in a similar way as CH-DAV and CH-AWS. In fair weather conditions winds at slope sites (Fig. S4) typically rotate clockwise when on the right sidewall of a valley (i.e, facing down-valley) and counterclockwise on the left sidewall, as winds undergo their diurnal transitions from along-valley to along-slope wind systems (Whiteman, 2000). Thus, the inclusion of slope sites in our analysis would confound our analysis of the wind turning associated with the shadow eclipse passage. The sites classified as "slope sites" (Table S3) turned out to be embedded in rather complex terrain for which it was impossible to make a credible reasonable prediction which rotation should be expected. Consequently, we focus primarily on the sites not located on slopes in the following analysis.

The wind direction effect during the eclipse observed at the 165 MeteoSwiss sites included both anticyclonic and cyclonic changes (Fig. 8, green bars). If slope sites are were excluded from the analysis, then a rather clear dominance of the cyclonic effect is was seen (68.7% of the remaining 112 sites; Fig. 8, black bars). In comparison to conditions during the same time of day on the day before the eclipse, the directional changes were mostly in the range –30° to –45° during the period from the first contact to maximum occultation (Fig. 8). Large direction changes exceeding –75° were less frequent than on the reference day before the eclipse.

The effect of the penumbral shading on wind direction at 10 m a.g.l. shows showed a strong dependence on site elevation. Figure 9 shows showed an elevational integration of the percentage of sites showing cyclonic influence during the penumbral shading as expected according to Aplin and Harrison (2003) (Fig. 1b). There is was only one elevation zone (1708–2730 m a.s.l., 14 sites) in which a significant cyclonic rather than anticyclonic influence ($p<0.05$ according to bootstrapped uncertainty bounds) was found. The eclipse effect seen at the sites in this elevation zone is was clearly in support of the revised theory by Aplin and Harrison (2003), which reduced the extent of the anticyclonic outflow around the umbra from ≈2400 km Clayton (1901) to ≈1600 km (Fig. 1). Interestingly, however, Hanna et al. (2016) did not find any discernible effect of this eclipse on wind directions in the UK and Iceland, and thus deduce deduced that there was no evidence of an eclipse cyclone. In contrast to Switzerland, the UK observed a fair share of cloudiness (see satellite imagery in Hanna et al., 2016) which may have muted

some meteorological responses to the occultation, as Burt (2016) noted. But ~~if the analysis is~~ when the analysis was constrained to sites with clear-sky conditions, Gray and Harrison (2016) found a clear cyclonic effect of approximately 20–40° in the comparison of surface measurements with forecast model simulations which were ignorant of the eclipse. ~~Which~~ While such a cyclonic effect is what would be expected for Switzerland following the theory ~~by~~ of Aplin and Harrison (2003), it contradicts ~~that~~ this theory for the geographic location of the British Islands~~, which should observe~~ . Here, anticyclonic modification of the wind direction should have been observed under both Clayton (1901) and Aplin and Harrison (2003) theories. Hence, Gray and Harrison (2016) offer a new interpretation similar to the nocturnal low level jet. This interpretation is however not likely to explain conditions in the complex terrain ~~fo~~ for the Swiss Alps ~~, and hence~~ because low level jets develop primarily on the Swiss Plateau (Ihly, 1995), not in the Alpine valleys. Hence we did not further adopt this interpretation here.

3.5 Spatial patterns of wind direction effects

Wind direction effects were spatially interpolated with ordinary Kriging using the krige.conv function of the geoR package of R. The partial sill parameter was set to 300°, and the range parameter was set to 1000 km. We tested the range 90°–300° for the partial sill setting, and 10–10,000 km for the range setting. The results were similar due to the optimization method used in Kriging and differed only in very minor details (see examples in our response, doi:10.5194/acp-2017-321-AC2). The selection for the final computations was thus based only on the facts that a 300° (or –60°) corresponded to the typical deviation angle of wind directions under cyclonic influence, and that 1000 km covered the entire domain of Switzerland.

To test if there ~~exists~~ existed a geographically consistent pattern of wind direction changes across Switzerland and Liechtenstein we performed a spatial interpolation (Fig. 10). For the reasons given above, we again focused on sites that ~~are~~ were not located on slopes (Fig. 10b). The resulting map, however, is relatively similar to the one using all sites (Fig. 10a).

If all stations ~~are~~ were considered irrespective of their individual topographic environment (Fig. 10a), then a complex pattern ~~emerges that does~~ emerged that did not show a clear spatial structure that could be related to the passing of the penumbral shadow. Also valley bottom sites (Fig. 10e) ~~show~~ showed a mixture of anticyclonic effects in the west, south of the Alps, and eastern Switzerland, with cyclonic effects seen between these three anticyclonic areas. Sites on flat ground without clear topographic influences (Fig. 10c) ~~show~~ showed cyclonic effects in the center of Switzerland, surrounded by anticyclonic effects namely in the Valais (southwestern Switzerland) and the northeast. Mountain top and hilltop sites (Fig. 10d) ~~show~~ showed yet another pattern, with anticyclonic influences seen mostly in the western half of Switzerland and cyclonic effects in the eastern half. The only group of sites showing a consistent spatial pattern ~~are~~ were those in the elevation range 1708–2730 m a.s.l. (Fig. 10f), the ranges with a statistically significant preference for cyclonic effects in Figure 9. This cyclonic effect ~~is~~ was seen across most of Switzerland, with the exception of a few high mountain sites in the Grisons (eastern Switzerland), the part of the study domain that ~~is~~ was farthest away from the trajectory of the eclipse (Fig. 1). This ~~elevation range corresponds to the elevation range~~ high elevation range corresponded to the level where the influence of the topographical roughness of the Swiss mountains ~~vanishes~~ vanished in vertical radiosonde profiles (at ≈2500 m, Wanner and Furger, 1990).

Taken together, these findings ~~lend support to~~ support the hypothesis that Switzerland was in the cyclonic part of the penumbral shading as expected from the Aplin and Harrison (2003) theory (Fig. 1b), and not within the anticyclonic part as would be

expected from the Clayton (1901) theory (Fig. 1a). Although no theory exists on how the transition zone between the inner anticyclonic and the outer cyclonic ring around the umbra should affect local wind directions, our analysis ~~indicates~~ indicated that the effect ~~is~~ was most likely a combination of distance from the center combined with the meso- and micro-scale topography around the site. This is not unexpected if the net effect of the shading is weak. The fact that there ~~is~~ was a significant preference for cyclonic effects at sites in the elevation range 1708–2730 m a.s.l., whereas there ~~is~~ was no significant difference between anticyclonic and cyclonic effects at other elevations, ~~suggests~~ suggested that the reduced dimensions of the anticyclonic band around the umbra as ~~suggested~~ proposed by Aplin and Harrison (2003) is more likely to be correct than the original Clayton (1901) model, in which Switzerland should have experienced a shift from cyclonic to anticyclonic influence as the occultation progressed towards its local maximum.

3.6 Comparison with findings from other eclipses

The present study expands ~~upon~~ previously published analyses of the eclipse effect using multiple stations in a given region. For example Brazel et al. (1993) performed a similar analysis of temperature effects using 16 weather stations in the Phoenix, Arizona, metropolitan area, but were unable to analyse wind direction effects. They ~~mention~~ mentioned two reasons why this was not feasible: (1) the eclipse occured in the morning when the wind flow tends to reverse due to topographic heating in the Salt River Valley, and (2) several of the available stations did not record wind direction, but only wind speed. The first point (given with reference to Frenzel, 1963) is typical for any topographically varying region on the globe and exactly matches the conditions experienced in this study. This effect was also emphasized by Anderson (1999), Vogel et al. (2001), and Sjöblom (2010): ~~the~~ surface cooling can trigger downslope and katabatic winds in mountainous regions, such as the Alps, the Arctic islands and Antarctica.

On 18 to 20 March 2015, synoptic pressure conditions over the European Alps showed a persistent high-pressure band between the UK and Russia, providing an excellent basis for comparing conditions during the solar eclipse with previous days. Although such comparisons are one of the most used approaches to quantify the effects of solar eclipses (Owen and Jones, 1927; Shur, 1984; Brazel et al., 1993; Jain et al., 1997; Dutta et al., 1999; Dolas et al., 2002; Gorchakov et al., 2007; Chernogor, 2008; Gorchakov et al., 2008; Sjöblom, 2010; Bala Subrahamanyam and Anurose, 2011; Bala Subrahamanyam et al., 2011; Muraleedharan et al., 2011; Bala Subrahamanyam et al., 2012; Murthy et al., 2013), in most cases weather conditions are rather variable and nonideal for direct comparisons. In Switzerland, the 20 March 2015 eclipse occurred when snow cover was disappearing at ~~montane~~ mountain locations around 1000 m a.s.l., and thus air temperatures varied more strongly from day to day than what would be desirable for estimating temperature effects. Therefore, we employed the less widely used approach by Segal et al. (1996) to fit a curvilinear interpolation over the period of occultation from first to fourth contact. This approach is typical for assessing effects on atmospheric constituents such as ozone (Tzanis et al., 2008). A third approach to deal with the variability of measurements during reference days is to take the 30-day hourly median values for comparison (Gerasopoulos et al., 2008). All three approaches have advantages and disadvantages. In our case, the direct comparison with the day before the eclipse during which similar synoptic weather conditions persisted would have led to a more pronounced temperature drop by an additional 1.3 K on average. The relationship between the temperature drop of all sites reported in Table S2 as used in

our study and the absolute difference to the day before the eclipse was

$$\Delta T_{19} = -2.06 \pm 0.17 + (0.48 \pm 0.09)\Delta T\,, \tag{5}$$

with ΔT being the temperature drop used in this study and ΔT_{19} being the alternative calculation of ΔT as the difference between the measurements made on 20 March and the same time of day on 19 March (the day before the eclipse; $p < 0.001$, adj. $R^2 = 0.124$).

The choice of method to determine the temperature drop—and any other variable of interest affected by the penumbral shading—has a substantial effect on the result, not only in our study, but also in other published results (e.g. Table 1). Only 9% of the ~~studies considered have~~ published studies reported stronger temperature effects than the most extreme 5.8 K drop at the Sorniot–Lac Inférier site reported here, although most temperature drop reports in the literature relate to ~~full~~ maximum occultation during total and annular eclipses. ~~With~~ During future eclipses it may now become possible to engage citizen scientists to determine the temperature drop during an eclipse and relate it to the probability distribution presented in Table 3 or to the Gamma distribution of Eq. (4) and Table 2, which would ~~allow them to~~ put their measurements into context (see also Portas et al., 2016; Barnard et al., 2016).

Differences in temperature drops among different eclipse events ~~are expected to depend on~~ depend on the solar elevation at the time of the eclipse (Reynolds, 1937). Here we showed that although the eclipse happened in the morning hours and although occultation was only partial ~~at all sites in~~ across Switzerland, substantial drops in air temperatures at several Swiss sites (Table S2) exceeded those observed at other locations with higher solar angles (Table 1). Thus, our results suggest that the topographic setting, not the geographic position on the globe, may actually be the most important determinant of the temperature drop for individual sites.

With respect to wind direction effects~~only~~, few studies are available for comparison, with Clayton (1901) still being a classical reference after more than one century. Regional weather forecast models are now run at a spatial resolution that should theoretically allow simulations of the effect of penumbral shading on wind speed (not assessed here due to inconsistent variability among the sites) and wind direction (as presented in Fig. 10). Gray and Harrison (2012) followed this approach for the southern UK during the 11 August 1999 eclipse, but found that the umbral shading did not produce clear effects on wind vectors. They concluded that the primary response of the model was restricted to ~~temperatures~~temperature. Similarly, Prenosil's (2000) simulations for Central Europe showed model responses for temperature and humidity, but not for near-surface winds. Few wind observations are available for testing of such models, and Prenosil (2000) concluded that special observation campaigns with very accurate sensors would be required to make progress. The six Swiss FluxNet sites ~~provide~~ provided detailed measurements, and many more sites are available globally via Fluxnet (Baldocchi et al., 2001). However, the Fluxnet sites provide only aggregated 30-minute averages, not the raw data at original resolution. Of our six sites with available high-frequency measurements, two sites (CH-DAV and CH-AWS, Fig. 7) showed a clear wind direction effect during the penumbral shading, even though the distance to the center of the eclipse was on the order of 2000 km.

4 Conclusions

Temperature responses to the eclipse were quite strong (up to 5.8 K cooling, 1.51 ± 0.02 K on average), especially in basin topography where the cold air from the occultation can pool. Our results suggest that the topographic setting ~~is~~ was the most important determinant of the temperature drop for individual sites. Effects on wind directions were variable and site-specific as well. Thermo-topographic winds generated in the penumbral zone of a solar eclipse can modify local wind systems, either by delaying of the onset of the diurnal wind shift (as seen at the CH-DAV site) or by preventing the establishment of an up-valley wind in mountainous areas (at the CH-AWS site). These effects can occur at a considerable distance from the umbral path and two theories exist on the wind direction effect at a distance of ≈2000 km from the center of the eclipse (Fig. 1). According to Clayton (1901), an anticyclonic outflow should extend up to 2400 km from the center of the eclipse, which would include all of Switzerland during the 20 March 2015 eclipse. The modified theory by Aplin and Harrison (2003) reduces this extent to 1600 km, which would exclude all of Switzerland during the 20 March 2015 eclipse and leave it in the outermost ring with cyclonic counterflow. Our ~~analysis indicates a significant preference for the latter , reduced dimensions,~~ analyses more strongly supported the latter theory, at least for the elevation range 1706–2750 m a.s.l. (the elevations at which the typical influence of the roughness of the mountain topography ~~tends~~ tended to vanish). In this elevation zone, the influence of the penumbral shading on near-surface wind directions ~~is~~ was detectable even at distances greater than 2000 km from the center of the umbra, at places where maximum occultation during an eclipse ~~is~~ was as low as 66–70%.

5 Data availability

Our data policy is available under http://www.gl.ethz.ch/research/data-archive.html. Aggregated Swiss FluxNet data are directly available from the European Flux Database Cluster (http://gaia.agraria.unitus.it/pi-area; 30-min averages). Binary raw data files, ancillary data at finer resolution than 30-min, and phenological camera images are available from the corresponding author on request. The MeteoSwiss data are directly available via their IDAWEB interface (https://gate.meteoswiss.ch/idaweb?language=en; registration required; freely available for non-commercial research projects).

Author contributions. WE designed the study, carried out all analyses, wrote and revised the manuscript. CDW provided essential topo-climatological input and advice for the analyses. All co-authors were involved in writing and contributed to the article with feedback and critique.

Competing interests. None.

Acknowledgements. This study made extensive use of standard meteorological data collected by MeteoSwiss, the Swiss Federal Office for Meteorology and Climatology, which also contains sites from the Swiss Airforce (Kdo LVb FULW 34) and the Swiss Federal Research

Institute WSL. We acknowledge the use of these data via the IDAWEB online database. We thank Jon Eugster, University of Zurich, for mathematical support with probability distribution model implementation. The Swiss National Science Foundation (SNF) supported research at the CH-OE2 Swiss FluxNet site via grant 146373, at the CH-DAV site via grant 148992 (~~ICOS~~ICOS-CH), and at the CH-CHA and CH-FRU sites via grant 154245.

References

Anderson, J.: Meteorological changes during a solar eclipse, Weather, 54, 207–215, 1999.

Anderson, R. C. and Keefer, D. R.: Observation of the temperature and pressure changes during the 30 June 1973 solar eclipse, J. Atmos. Sci., 32, 228–231, 1975.

Anderson, R. C., Keefer, D. R., and Myers, O. E.: Atmospheric pressure and temperature changes during the 7 March 1970 solar eclipse, J. Atmos. Sci., 29, 583–587, 1972.

Anonymous: Meteorological Observations during the Solar Eclipse of 30th November, Boston Medical and Surgical Journal, 11, 295–296, 1834.

Aplin, K. and Harrison, R.: Meteorological effects of the eclipse of 11 August 1999 in cloudy and clear conditions, Proc. R. Soc. Lond. A, 459, 353–371, doi:10.1098/rspa.2002.1042, 2003.

Aplin, K. L., Scott, C. J., and Gray, S. L.: Atmospheric changes from solar eclipses, Phil. Trans. R. Soc. A, 374, 20150 217, doi:10.1098/rsta.2015.0217, 2016.

Ashworth, J.: Fall of temperature during the solar eclipse, Nature, 120, 227, 1927.

Bala Subrahamanyam, D. and Anurose, T.: Solar eclipse induced impacts on sea/land breeze circulation over Thumba: A case study, J. Atmos. Sol. Terr. Phys., 73, 703–708, doi:10.1016/j.jastp.2011.01.002, 2011.

Bala Subrahamanyam, D., Anurose, T., Mohan, M., Santosh, M., Kiran Kumar, N. V. P., Sijikumar, S., Prijith, S. S., and Aloysius, M.: Atmospheric surface-layer response to the annular solar eclipse of 15 January 2010 over Thiruvananthapuram, India, Bound.-Layer Meteorol., 141, 325–332, doi:10.1007/s10546-011-9627-z, 2011.

Bala Subrahamanyam, D., Anurose, T., Mohan, M., Santosh, M., Kiran Kumar, N., and Sijikumar, S.: Impact of annular solar eclipse of 15 January 2010 on the atmospheric boundary layer characteristics over Thumba: A case study, Pure Appl. Geophys., 169, 741–753, doi:10.1007/s00024-011-0336-9, 2012.

Baldocchi, D., Falge, E., Gu, L., Olson, R., Hollinger, D., Running, S., Anthoni, P., Bernhofer, C., Davis, K., Evans, R., Fuentes, J., Goldstein, A., Katul, G., Law, B., Lee, X., Malhi, Y., Meyers, T., Munger, W., Oechel, W., Paw U, K. T., Pilegaard, K., Schmid, H. P., Valentini, R., Verma, S., Vesala, T., Wilson, K., and Wofsy, S.: FLUXNET: A new tool to study the temporal and spatial variability of ecosystem-scale carbon dioxide, water vapor, and energy flux densities, Bull. Am. Meteorol. Soc., 82, 2415–2434, 2001.

Barnard, L., Portas, A. M., Gray, S. L., and Harrison, R. G.: The National Eclipse Weather Experiment: an assessment of citizen scientist weather observations, Phil. Trans. R. Soc. A, 374, 20150 220, doi:10.1098/rsta.2015.0220, 2016.

Bilham, E. G.: Meteorological observations during the annular solar eclipse of April 8th 1921, Q. J. R. Meteorol. Soc., 47, 206–210, doi:10.1002/qj.49704719907, 1921.

Boucher, O., Randall, D., Artaxo, P., Bretherton, C., Feingold, G., Forster, P., Kerminen, V.-M., Kondo, Y., Liao, H., Lohmann, U., Rasch, P., Satheesh, S. K., Sherwood, S., Stevens, B., and Zhang, X. Y.: Clouds and Aerosols, In: Stocker T. F., Qin D., Plattner G.-K., Tignor M., Allen S. K., Boschung J., Nauels A., Xia Y., Bex V. and Midgley P. M. (eds.), Climate Change 2013: The Physical Science Basis. Contribution of Working Group I to the Fifth Assessment Report of the Intergovernmental Panel on Climate Change, Cambridge University Press, Cambridge, United Kingdom and New York, NY, USA, 2013.

Brazel, A., Cerveny, R., and Trapido, B.: Localized climatic responses during the 11 July 1991 eclipse: Phoenix AZ, Climatic Change, 23, 155–168, doi:10.1007/BF01097335, 1993.

Burt, S.: Meteorological responses in the atmospheric boundary layer over southern England to the deep partial eclipse of 20 March 2015, Phil. Trans. R. Soc. A, 374, 20150214, doi:10.1098/rsta.2015.0214, 2016.

Chernogor, L.: Effects of solar eclipses in the surface atmosphere, Izvestiya – Atmos. Ocean Phys., 44, 432–447, doi:10.1134/S000143380804004X, 2008.

Clark, M. R.: On the variability of near-surface screen temperature anomalies in the 20 March 2015 solar eclipse, Phil. Trans. R. Soc. A, 374, 20150213, doi:10.1098/rsta.2015.0213, 2016.

Clayton, H. H.: The eclipse cyclone and the diurnal cyclones, Annals of the Astronomical Observatory of Harvard College, 18, 1–31, 1901.

Dolas, P. M., Ramchandran, R., Gupta, K. S., Patil, S. M., and Jadhav, P. N.: Atmospheric surface-layer processes during the total solar eclipse of 11 August 1999, Bound.-Layer Meteorol., 104, 445–461, 2002.

Dutta, G., Joshi, M., Pandarinath, N., Bapiraju, B., Srinivasan, S., Subba Rao, J., and Aleem Basha, H.: Wind and temperature over Hyderabad during the solar eclipse of 24 Oct. 1995, Indian J. Radio Space Phys., 28, 11–14, 1999.

Economou, G., Christou, E., Giannakourou, A., Gerasopoulos, E., Georgopoulos, D., Kotoulas, V., Lyra, D., Tsakalis, N., Tzortziou, M., Vahamidis, P., Papathanassiou, E., and Karamanos, A.: Eclipse effects on field crops and marine zooplankton: The 29 March 2006 total solar eclipse, Atmos. Chem. Phys., 8, 4665–4676, 2008.

Efron, B.: Bootstrap methods: another look at the jackknife, The Annals of Statistics, 7, 1–26, 1979.

Fernández, W., Castro, V., and Hidalgo, H.: Air temperature and wind changes in Costa Rica during the total solar eclipse of July 11, 1991, Earth, Moon, and Planets, 63, 133–147, doi:10.1007/BF00575102, 1993a.

Fernández, W., Castro, V., Wright, J., Hidalgo, H., and Sáenz, A.: Changes in solar irradiance and atmospheric turbidity in Costa Rica during the total solar eclipse of July 11, 1991, Earth, Moon, and Planets, 63, 119–132, doi:10.1007/BF00575101, 1993b.

Fernández, W., Hidalgo, H., Coronel, G., and Morales, E.: Changes in meteorological variables in Coronel Oviedo, Paraguay, during the total solar eclipse of 3 November 1994, Earth, Moon and Planets, 74, 49–59, 1996.

Ferrel, W.: A Popular Treatise on the Winds, John Wiley, New York, 2 edn., https://archive.org/details/cu31924003877606, 1890.

Founda, D., Melas, D., Lykoudis, S., Lisaridis, I., Gerasopoulos, E., Kouvarakis, G., Petrakis, M., and Zerefos, C.: The effect of the total solar eclipse of 29 March 2006 on meteorological variables in Greece, Atmos. Chem. Phys., 7, 5543–5553, 2007.

Frenzel, C. W.: The wind regime at Tucson and Phoenix and their relation to air pollution, J. AZ-NV Acad. Sci., 2, 98–103, 1963.

Gerasopoulos, E., Zerefos, C., Tsagouri, I., Founda, D., Amiridis, V., Bais, A., Belehaki, A., Christou, N., Economou, G., Kanakidou, M., Karamanos, A., Petrakis, M., and Zanis, P.: The total solar eclipse of March 2006: Overview, Atmos. Chem. Phys., 8, 5205–5220, 2008.

Good, E.: Satellite observations of surface temperature during the March 2015 total solar eclipse, Phil. Trans. R. Soc. A, 374, 20150219, doi:10.1098/rsta.2015.0219, 2016.

Gorchakov, G., Kadygrov, E., Isakov, A., Karpov, A., and Miller, E.: Influence of a solar eclipse on thermal stratification and the turbulence regime, Dokl. Earth Sci., 417, 1243–1246, doi:10.1134/S1028334X07080259, 2007.

Gorchakov, G., Kadygrov, E., Kortunova, Z., Isakov, A., Karpov, A., Kopeikin, V., and Miller, E.: Eclipse effects in the atmospheric boundary layer, Izvestiya – Atmos. Ocean Phys., 44, 100–106, doi:10.1007/s11485-008-1011-z, 2008.

Gray, S. and Harrison, R.: Diagnosing eclipse-induced wind changes, Proc. R. Soc. Lond. A, 468, 1839–1850, doi:10.1098/rspa.2012.0007, 2012.

Gray, S. L. and Harrison, R. G.: Eclipse-induced wind changes over the British Isles on the 20 March 2015, Phil. Trans. R. Soc. A, 374, 20150224, doi:10.1098/rsta.2015.0224, 2016.

Gross, P. and Hense, A.: Effects of a total solar eclipse on the mesoscale atmospheric circulation over Europe – A model experiment, Meteorol. Atmos. Phys., 71, 229–242, 1999.

Hanna, E., Penman, J., Jónsson, T., Bigg, G. R., Björnsson, H., Sjúrðarson, S., Hansen, M. A., Cappelen, J., and Bryant, R. G.: Meteorological effects of the solar eclipse of 20 March 2015: analysis of UK Met Office automatic weather station data and comparison with automatic weather station data from the Faroes and Iceland, Phil. Trans. R. Soc. A, 374, 20150 212, doi:10.1098/rsta.2015.0212, 2016.

Harrison, R. G. and Hanna, E.: Introduction: The solar eclipse: a natural meteorological experiment, Phil. Trans. R. Soc. A, 374, 20150 225, doi:10.1098/rsta.2015.0225, 2016.

Hayes, R.: Fall in air temperature during the solar eclipse of December 13–14, 1936, Nature, 139, 967–968, 1937.

Hurni, L., ed.: Atlas of Switzerland, Version 3, Swisstopo, Wabern–Bern, CD-ROM edn., www.atlasofswitzerland.ch, 2010.

Ihly, B.: Der grossräumige nordöstliche Jet in der unteren Troposphäre im Schweizer Mittelland, Lenticularis Verlag, Opfikon, Switzerland, 108 pp., 1995.

Jain, S., Arya, B., Singh, S., Tripathi, O., and Hamid, A.: Measurement of various atmospheric parameters during a total solar eclipse, Terrestrial, Atmospheric and Oceanic Sciences, 8, 371–384, 1997.

Johns, M. V.: Importance sampling for bootstrap confidence intervals, Journal of the American Statistical Association, 83, 709–714, 1988.

Leeds-Harrison, P., Youngs, E., and Blackburn, D.: Soil temperatures during the solar eclipse on 11 August 1999, Eur. J. Soil Sci., 51, 183–184, doi:10.1046/j.1365-2389.2000.00293.x, 2000.

Mauder, M., Desjardins, R., Oncley, S., and MacPherson, I.: Atmospheric response to a partial solar eclipse over a cotton field in Central California, J. Appl. Meteorol. Climatol., 46, 1792–1803, doi:10.1175/2007JAMC1495.1, 2007.

Menke, D. H.: Total eclipse over Karimata: An astronomical and meteorological event, Weatherwise, 41, 272–275, doi:10.1080/00431672.1988.9925277, 1988.

MeteoSwiss: Klimabulletin März 2015 (climate bulletin, in German only), http://www.meteoschweiz.admin.ch/content/dam/meteoswiss/de/Klima/Gegenwart/Klima-Berichte/doc/klimabulletin_maerz_2015.pdf, accessed 2017-10-06, 2015.

MeteoSwiss: SwissMetNet, the automatic monitoring network of MeteoSwiss, http://www.meteoswiss.admin.ch/home/measurement-and-forecasting-systems/land-based-stations/automatisches-messnetz.html, accessed 2017-01-05, 2017.

Michna, P., Eugster, W., Hiller, R., Zeeman, M. J., and Wanner, H.: Topoclimatological case-study of Alpine pastures near the Albula Pass in the eastern Swiss Alps, Geogr. Helv., 68, 249–263, doi:10.5194/gh-68-249-2013, 2013.

Mill, H. R.: Air temperature during the solar eclipse, Nature, 54, 391, 1896.

Muraleedharan, P., Nisha, P., and Mohankumar, K.: Effect of January 15, 2010 annular solar eclipse on meteorological parameters over Goa, India, J. Atmos. Sol. Terr. Phys., 73, 1988–1998, doi:10.1016/j.jastp.2011.06.003, 2011.

Murthy, B., Latha, R., Sreeja, P., and Dharmaraj, T.: Transient land breeze: Eclipse induced wind flow modifications-Observations over plant canopy, J. Atmos. Sol. Terr. Phys., 89, 33–39, doi:10.1016/j.jastp.2012.07.010, 2013.

NASA: https://eclipse.gsfc.nasa.gov/SEplot/SEplot2001/SE2015Mar20T.GIF, accessed: 2017-01-05, 2015.

NASA: Javascript Solar Eclipse Explorer, https://eclipse.gsfc.nasa.gov/JSEX/JSEX-EU.html, accessed: 2017-01-05, 2017.

Nufer, R. and Gfeller, P.: Messung der Lufttemperature während der totalen Sonnenfinsternis am 26. Februar 1998 bei Sinamaica (Venezuela), Orion, 286, 28, 1998.

Nymphas, E., Adeniyi, M., Ayoola, M., and Oladiran, E.: Micrometeorological measurements in Nigeria during the total solar eclipse of 29 March, 2006, J. Atmos. Sol. Terr. Phys., 71, 1245–1253, doi:10.1016/j.jastp.2009.04.014, 2009.

Owen, E. A. and Jones, H. I.: Potentials during the solar eclipse, Nature, 120, 120, doi:10.1038/120120a0, 1927.

Pasachoff, J.: Solar eclipses as an astrophysical laboratory, Nature, 459, 789–795, doi:10.1038/nature07987, 2009.

Pasachoff, J. M., Peñaloza-Murillo, M. A., Carter, A. L., and Roman, M. T.: Terrestrial atmospheric responses on Svalbard to the 20 March 2015 Arctic total solar eclipse under extreme conditions, Phil. Trans. R. Soc. A, 374, 20160 188, doi:10.1098/rsta.2016.0188, 2016.

Penaloza-Murillo, M. and Pasachoff, J.: Air-cooling mathematical analysis as inferred from the air-temperature observation during the 1st total occultation of the Sun of the 21st century at Lusaka, Zambia, J. Atmos. Sol. Terr. Phys., 125–126, 59–77, doi:10.1016/j.jastp.2015.02.002, 2015.

Pleijel, H.: Observations of temperature and air humidity during the total solar eclipse 29 March 2006 at Side, Turkey, Meteorol. Z., 18, 107–109, doi:10.1127/0941-2948/2008/0324, 2009.

Portas, A. M., Barnard, L., Scott, C., and Harrison, R. G.: The National Eclipse Weather Experiment: use and evaluation of a citizen science tool for schools outreach, Phil. Trans. R. Soc. A, 374, 20150 223, doi:10.1098/rsta.2015.0223, 2016.

Prenosil, T.: The influence of the 11 August 1999 total solar eclipse on the weather over central Europe, Meteorol. Z., 9, 351–359, 2000.

R Core Team: R: A Language and Environment for Statistical Computing, R Foundation for Statistical Computing, Vienna, Austria, https://www.R-project.org/, 2016.

Reynolds, J. H.: Proceedings of the Meeting of the Royal Astronomical Society, The Observatory, 60, 1–8, 1937.

Segal, M., Turner, R., Prusa, J., Bitzer, R., and Finley, S.: Solar eclipse effect on shelter air temperature, Bull. Amer. Meteor. Soc., 77, 89–99, 1996.

Shur, G.: Aircraft investigation of the effect of a total solar eclipse on temperature, wind, and turbulence in the atmosphere, Soviet Meteorol. Hydrol., 6, 31–34, 1984.

Sjöblom, A.: A solar eclipse seen from the High Arctic during the period of midnight sun: Effects on the local meteorology, Meteorol. Atmos. Phys., 107, 123–136, doi:10.1007/s00703-010-0070-3, 2010.

Stoev, A., Stoeva, P., Kiskinova, N., and Stoyanov, N.: Evolution of the basic micrometeorological parameters during the total solar eclipse of 29 March 2006 at Manavgat, Turkey, Proc. of SPIE, 6936, doi:10.1117/12.783768, 2008.

Szalowski, K.: The effect of the solar eclipse on the air temperature near the ground, J. Atmos. Sol. Terr. Phys., 64, 1589–1600, doi:10.1016/S1364-6826(02)00134-7, 2002.

Tzanis, C., Varotsos, C., and Viras, L.: Impacts of the solar eclipse of 29 March 2006 on the surface ozone concentration, the solar ultraviolet radiation and the meteorological parameters at Athens, Greece, Atmos. Chem. Phys., 8, 425–430, doi:10.5194/acp-8-425-2008, 2008.

Venkat Ratnam, M., Shravan Kumar, M., Basha, G., Anandan, V., and Jayaraman, A.: Effect of the annular solar eclipse of 15 January 2010 on the lower atmospheric boundary layer over a tropical rural station, J. Atmos. Sol. Terr. Phys., 72, 1393–1400, doi:10.1016/j.jastp.2010.10.009, 2010.

Vogel, B., Baldauf, M., and Fiedler, F.: The influence of a solar eclipse on temperature and wind in the Upper-Rhine Valley – A numerical case study, Meteorologische Zeitschrift, 10, 207–214, doi:10.1127/0941-2948/2001/0010-0207, 2001.

Wanner, H. and Furger, M.: The Bise – Climatology of a regional wind north of the Alps, Meteorol. Atmos. Phys., 43, 105–115, doi:10.1007/BF01028113, 1990.

Ward, R. D.: Changes of temperature during the recent solar eclipse, Science, 4, 563, 1896.

Whiteman, C. D.: Mountain Meteorology: Fundamentals and Applications, Oxford University Press, New York, Oxford, 355 pp., 2000.

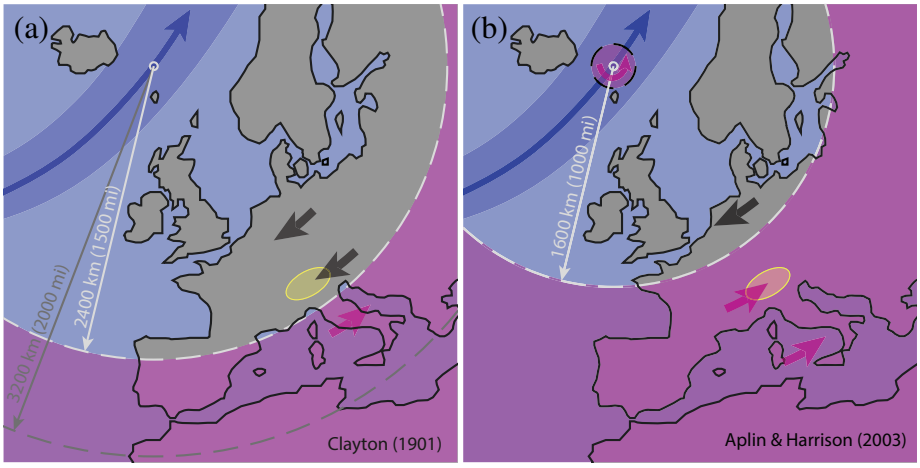

Figure 1. Theoretical effects of penumbral shading on wind direction. Wind directions around the center of the umbra (east of Iceland) according to the theory of Clayton (1901) (left) and Aplin and Harrison (2003) (right), schematically drawn for the time of maximum occultation over the Swiss Alps (yellow area). The eclipse trajectory is shown with a blue arrow, and the umbral path (100% occultation) is shown with a blueish band. The schematic shows the time of greatest eclipse with ~~it's~~ its center indicated by a gray circle.

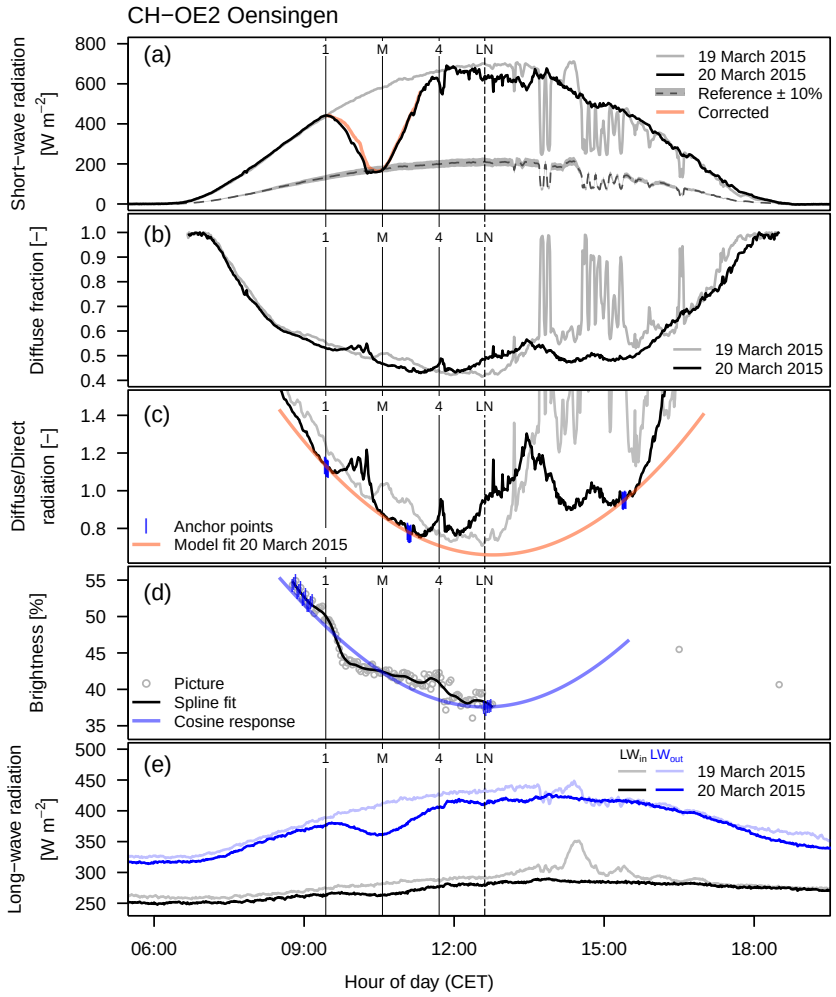

Figure 2. Radiation effects at the CH-OE2 Swiss FluxNet site. (a) Incoming short-wave radiation, (b) fraction of diffuse radiation, (c) ratio between diffuse and direct radiation, (d) evolution of brightness of the vegetation during the eclipse, and (e) long-wave radiation components. The four vertical lines indicate first contact (1), maximum occultation (M), last contact (4), and local noon (LN). Bold lines show the conditions during the day of the eclipse (black or darker color) in comparison with the preceding day (brighter color). The dashed reference curve in (a) is the measurement from 19 March 2015 multiplied ~~with~~ by 0.6996, the theoretical maximum occultation at the site (± 10% shown with a gray band). The fraction of diffuse radiation in (b) was measured with a quantum sensor measuring diffuse photosynthetic photon flux density (PPFD, 400–700 nm wavelength) in relation to total PPFD. The red model curve in (c) ~~was fitted~~ shows an empirical parabolic fit to the three periods with blue ~~datapoints~~ data points to ~~correct~~ obtain a reference for the correction of (a) for cloud passage during the eclipse (red line in (a)). The ~~blue curve~~ assumption made here is that the ratio of diffuse to direct PPFD is valid also for the entire wavelength spectrum of short-wave radiation shown in (a). During the penumbral shading phase, the phenological camera recorded images every 2 minutes, from which relative surface brightness was computed in the footprint area of the radiation measurements (gray symbols in (d)~~is a corresponding~~). The local polynomial regression fit (black line in (d)) shows a marked decrease in brightness after first contact in comparison to the ~~image data~~theoretical cosine response (blue line in (d), anchored at the pictures marked with vertical blue bars), followed by an almost constant brightness during the occultation phase. LW_{in} and LW_{out} in (e) are incoming and ~~outging~~ outgoing long-wave radiation, respectively. ~~See text for details.~~

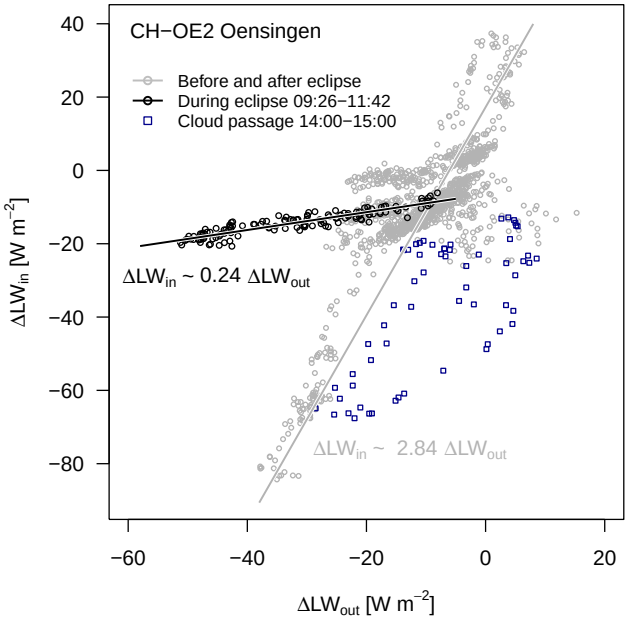

Figure 3. Long-wave back radiation effect during the eclipse (black symbols and regression line) in comparison to conditions before and after the eclipse (gray symbols and regression line). The differences ΔLW between 1-minute averages from the day before the eclipse and the same time during the day of the eclipse are shown (ΔLW_{in} in relation to ΔLW_{out} ~~; see Section 3.2, Eq. 3~~using the regression approach $\Delta LW_x = LW_x(\text{20 March}) - LW_x(\text{19 March})$ with x representing index $_{\text{in}}$ or $_{\text{out}}$). Measurements made during a period with cloud passage on 19 March 2015 (blue symbols) were excluded from analysis.

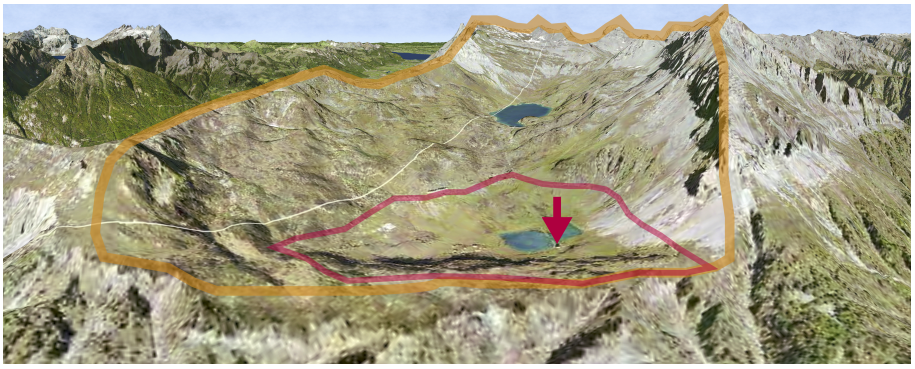

Figure 4. Oblique view of the surroundings of the Sorniot–Lac Inférieur de Fully weather station. The red arrow marks the location of the station, the red line marks the drainage area up to the lowest pass, and the orange line marks the full drainage area. The area was completely covered with snow and the lake was frozen during the eclipse. Imagery from Atlas of Switzerland V3 (Hurni, 2010), © 2016 swisstopo (JD100042).

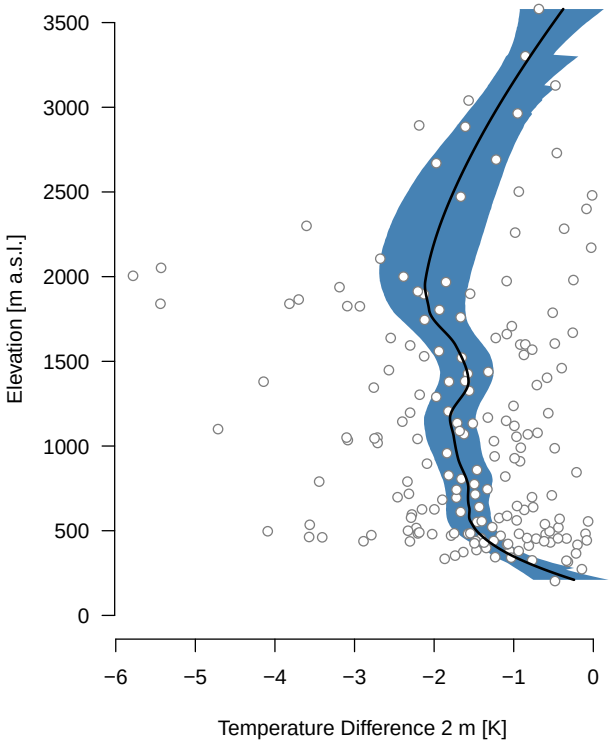

Figure 5. Temperature reduction maximum during the solar eclipse at 184 weather stations in Switzerland and Liechtenstein (open circles) that record 10-minute averages. The elevation profile (bold line showing the moving mean over a 350 m elevational window, equal to 10% of the entire elevation range) and its 95% confidence interval (blue band) were estimated using nonparametric bootstrapping. ~~See Section 2.2 and Table for details.~~

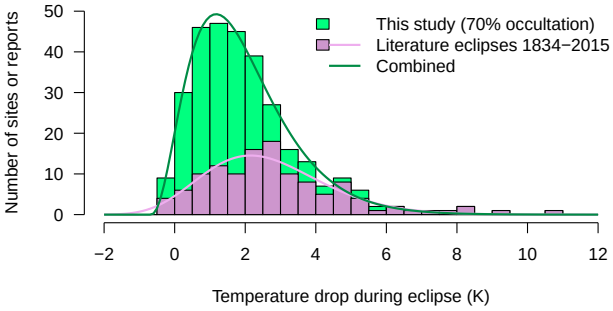

Figure 6. Histogram of temperature reduction at all sites included in this study and those reported in the literature. The stacked bars show number of sites of this study (green bars) on top of those for literature reports (violet bars). The solid lines show the best fit of the scaled probability distributions (Eq. 4, Table 2) of values reported in the literature (violet line) and the combination of literature data with values reported in this study (dark green line).

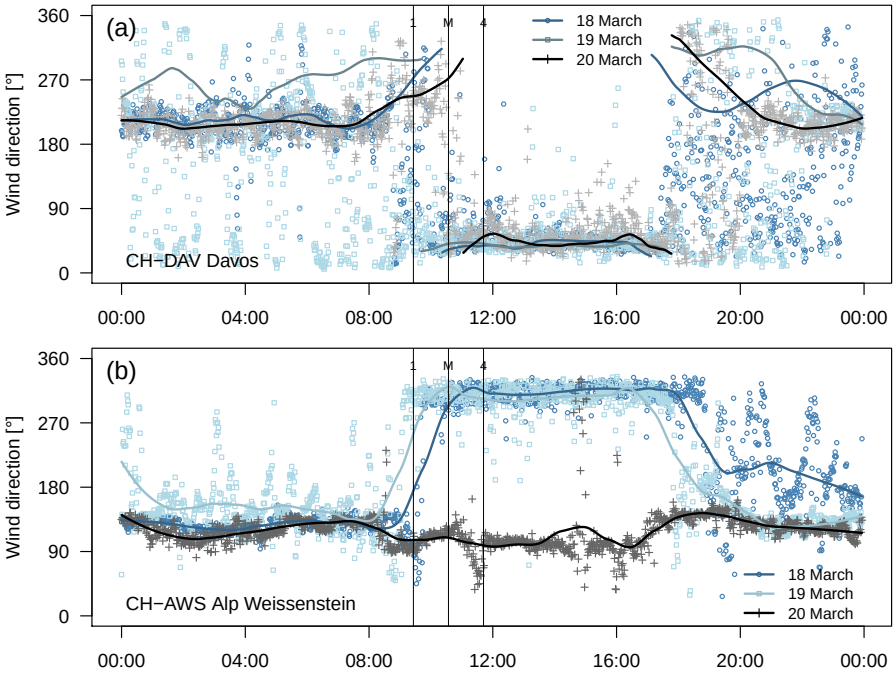

Figure 7. Wind direction as a function of time (a) at CH-DAV and (b) at CH-AWS on 18, 19 and 20 March, showing a delayed wind direction reversal at CH-DAV on 20 March (a), and a suppression of the typical wind reversal at CH-AWS on 20 March (b) ~~. From~~ determined from 1-minute average data. The bold lines are local polynomial regression (loess) fits.

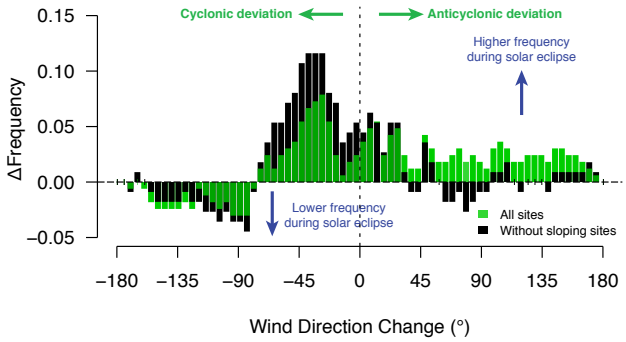

Figure 8. Deviation of wind direction changes (range –180° to 180°) during the eclipse expressed as Δ~~Probability~~ Frequency with respect to a random uniform distribution. The wind direction change is the difference between the first half of the eclipse in comparison with the corresponding time period on 19 March.

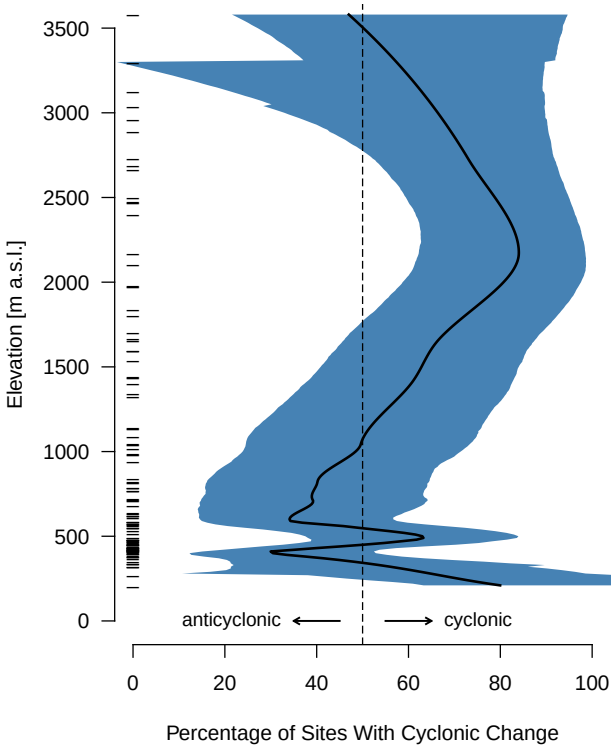

Figure 9. Elevation dependence of cyclonic and anticyclonic influences during penumbral shading. Using MeteoSwiss sites the percentage of sites showing cyclonic or anticyclonic effects was determined and elevational best estimates (bold line) and uncertainty of the estimate (90% confidence interval in blue) were estimated using nonparametric bootstrapping. The vertical dashed line at 50% indicates the insignificant random outcome. Each horizontal mark near the elevation axis represents one weather station.

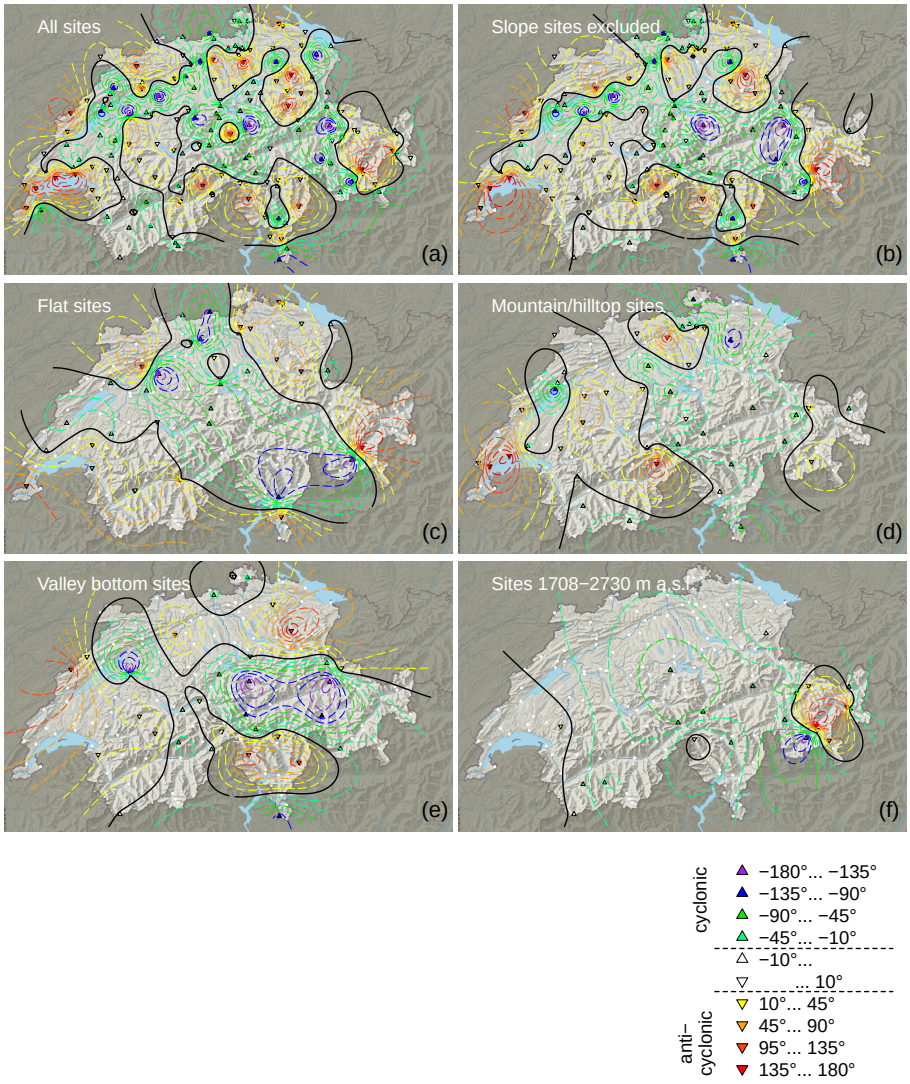

Figure 10. Spatial distribution of wind direction changes over Switzerland during the 20 March 2015 eclipse. Yellowish to reddish colors indicate anticyclonic rotation, while greenish to bluish colors indicate cyclonic rotation. The bold and broken isolines show lines of equal rotation angle at 20° intervals. The bold line separates areas with cyclonic from anticyclonic wind direction changes. Base map from Atlas of Switzerland V3 (Hurni, 2010), © 2016 swisstopo (JD100042).

Table 1. Compilation of literature reports on temperature drops during maximum occultation of the eclipse since 1834. Most reports are from total or annular eclipses, but a few studies also report values from partial eclipses or partial occultation at a given locality. More observations are tabulated in Aplin et al. (2016), but not all these reports allow the calculation of the temperature drop.

Date	Location | Additional Information	Temperature Drop	Reference
1834-11-30	Boston, Mass., USA	0.3 K	Anonymous (1834)
1896-08-09	Vadsö, Norway (70°04′ N)	1.0–1.6 K	Mill (1896)
1896-08-09	Vadsö, Norway (70°04′ N)	3.1 K	Ward (1896)
1905-08-30	Burgos	8.3 K	Reynolds (1937)
1918-06-08	Goldendale, Washington, USA	3.6 K	Anderson (1999)
1921-04-08	Bexley Heath	1.1 K	Bilham (1921)
1921-04-08	Bristol	4.2 K	Bilham (1921)
1921-04-08	Nottingham (Lenton Fields)	3.0 K	Bilham (1921)
1921-04-08	Prestou (Hoghton)	1.7 K	Bilham (1921)
1927-06-29	Bangor, UK	0.5 K	Owen and Jones (1927)
1927-06-29	English eclipse, cloudy	nothing remarkable	Reynolds (1937)
1927-06-29	Southport	0.5 K	Ashworth (1927)
1932-08-31	Canadian eclipse, cloudy	very small fall	Reynolds (1937)
1936-06-19	Chios	1 K	Reynolds (1937)
1936-06-19	Omsk	5 K	Reynolds (1937)
1936-06-19	on steam ship Strathaird	1.5 K	Reynolds (1937)
1936-06-19	Portugal	2.7–3.3 K	Reynolds (1937)
1936-12-13	New Plymouth, New Zealand	4.2 K	Hayes (1937)
1970-03-07	Lee, Florida, USA	3.2 K	Anderson et al. (1972)
1973-06-30	Chinguetti, Mauritania	3.5 K	Anderson and Keefer (1975)
1973-06-30	Chinguetti, Mauritania	2.5 K	Anderson and Keefer (1975)
1973-06-30	Chinguetti, Mauritania	2.5 K	Anderson and Keefer (1975)
1979-02-26	Hecla, Manitoba, Canada	2.0 K	Anderson (1999)
1984-05-30	'in Georgia'	7.8 K	Menke (1988)
1988-03-18	Ship, coast of Karimata island	2.2 K	Menke (1988)
1991-07-11	Agriculture/golf, wet fraction 1.00, albedo 0.20–0.25	1.40 K	Brazel et al. (1993)
1991-07-11	Costa Rica	no info	Fernández et al. (1993b)
1991-07-11	Costa Rica, Damas	4.7 K	Fernández et al. (1993a)
1991-07-11	Costa Rica, Fabio Baudrit Experimental Station	5.5 K	Fernández et al. (1993a)
1991-07-11	Costa Rica, Liberia, Alajuela and Palmar Sur	3.0–3.5 K	Fernández et al. (1993a)
1991-07-11	Costa Rica, Limón	3.0 K	Fernández et al. (1993a)
1991-07-11	Costa Rica, Puntarenas	2.7 K	Fernández et al. (1993a)
1991-07-11	Costa Rica, Santa Cruz and Filadelfia	2.0–2.5 K	Fernández et al. (1993a)
1991-07-11	Costa Rica, Tárcoles	8.5 K	Fernández et al. (1993a)

Date	Where | Additional Information	Temperature Drop	Reference
1991-07-11	Desert, wet fraction 0.00, albedo 0.27	2.65 K	Brazel et al. (1993)
1991-07-11	Fresno, California, USA, cotton field	ca. 4.5 K	Mauder et al. (2007)
1991-07-11	Industrial/airport, wet fraction 0.07, albedo 0.1	1.38 K	Brazel et al. (1993)
1991-07-11	Residential/commercial, wet fraction 0.47, albedo 0.20–0.25	1.93 K	Brazel et al. (1993)
1994-05-10	Ames, IA, USA	2.3 K	Segal et al. (1996)
1994-05-10	Boulder, CO, USA	2.2 K	Segal et al. (1996)
1994-05-10	Chicago, IL, USA	6.1 K	Segal et al. (1996)
1994-05-10	Estes Park, CO, USA	3.6 K	Segal et al. (1996)
1994-05-10	Ft. Collins, CO, USA	2.2 K	Segal et al. (1996)
1994-05-10	Keenesburg, CO, USA	3.0 K	Segal et al. (1996)
1994-05-10	Lakewood, CO, USA	2.7 K	Segal et al. (1996)
1994-05-10	Lamberton, MN, USA	3.1 K	Segal et al. (1996)
1994-05-10	Longmont, CO, USA	2.8 K	Segal et al. (1996)
1994-05-10	Loveland, CO, USA	3.3 K	Segal et al. (1996)
1994-05-10	Morris, MN, USA	2.3 K	Segal et al. (1996)
1994-05-10	Norman, OK, USA	3.6 K	Segal et al. (1996)
1994-05-10	Nowata, Oklahoma, USA	3.0 K	Anderson (1999)
1994-05-10	Nunn, CO, USA	1.9 K	Segal et al. (1996)
1994-05-10	Rollinsville, CO, USA	2.3 K	Segal et al. (1996)
1994-05-10	Sedalia, MO, USA	4.2 K	Segal et al. (1996)
1994-05-10	Springfield, IL, USA	6.1 K	Segal et al. (1996)
1994-05-10	St. Paul, MN, USA	1.5 K	Segal et al. (1996)
1994-05-10	Waseca, MN, USA	3.7 K	Segal et al. (1996)
1994-05-10	White Sands, New Mexico	5.5 K	Anderson (1999)
1994-05-10	White Sands, New Mexico	0.4 K	Anderson (1999)
1994-11-03	Coronel Oviedo, Paraguay	3.3 K	Fernández et al. (1996)
1995-10-24	Neem ka Thana, India	3 K	Jain et al. (1997)
1995-10-24	New Delhi, India	1.5 K	Jain et al. (1997)
1995-10-24	New Delhi, India	6–8 K	Jain et al. (1997)
1995-10-25	Hyderabad, India	9–10 K	Dutta et al. (1999)
1998-02-26	Sinamaica, Venezuela	5 K	Nufer and Gfeller (1998)
1999-08-11	Akola, Central India	1–2 K	Dolas et al. (2002)
1999-08-11	Kharkiv, Ukraine, max. occultation 0.73	7.3 K	Chernogor (2008)
1999-08-11	Modeling study, Central Europe	average 3.5 K	Gross and Hense (1999)
1999-08-11	Modeling study, Central Europe	peak up to 5 K	Gross and Hense (1999)
1999-08-11	Silsoe, Bedfordshire, UK, soil temperature at 10 mm depth	1.6 K	Leeds-Harrison et al. (2000)
1999-08-11	Silsoe, Bedfordshire, UK, under grass temperature	0.5 K	Leeds-Harrison et al. (2000)

Date	Where | Additional Information	Temperature Drop	Reference
1999-08-11	Southern UK	up to 3 K	Gray and Harrison (2012)
1999-08-11	Szczawnica, Poland	11 K	Szalowski (2002)
2001-06-21	Lusaka, Zambia	5.38 ± 0.04 K	Penaloza-Murillo and Pasachoff (2015)
2003-05-31	Kharkiv, Ukraine, max. occultation 0.64	2.1 K	Chernogor (2008)
2005-10-03	Kharkiv, Ukraine, max. occultation 0.24	1.3 K	Chernogor (2008)
2006-03-29	central Greece	2.7 K	Nymphas et al. (2009)
2006-03-29	Finokalia, Greece	2.3 K	Founda et al. (2007)
2006-03-29	Ibadan, Nigeria, 1 m	1.6 K	Nymphas et al. (2009)
2006-03-29	Ibadan, Nigeria, 12 m	0.8 K	Nymphas et al. (2009)
2006-03-29	Ibadan, Nigeria, 6 m	1 K	Nymphas et al. (2009)
2006-03-29	Kastelorizo, Greece	2.3 K	Founda et al. (2007)
2006-03-29	Kharkiv, Ukraine, max. occultation 0.77	2.3 K	Chernogor (2008)
2006-03-29	Kislovodsk, Russia	3 K	Gorchakov et al. (2008)
2006-03-29	Kislovodsk, Russia, 600 m a.s.l.	2 K	Gorchakov et al. (2007)
2006-03-29	Kislovodsk, Russia, surface atmospheric layer	3.4 ± 0.5 K	Gorchakov et al. (2007)
2006-03-29	Manavgat, Turkey	5 K	Stoev et al. (2008)
2006-03-29	Markopoulo (Athens), Greece	2.7 K	Founda et al. (2007)
2006-03-29	northern Greece	3.9 K	Nymphas et al. (2009)
2006-03-29	Palini (Athens), Greece	1.6 K	Founda et al. (2007)
2006-03-29	Penteli (Athens), Greece	2.7 K	Founda et al. (2007)
2006-03-29	Side, Turkey	5 K	Pleijel (2009)
2006-03-29	southern Greece	2.3 K	Nymphas et al. (2009)
2006-03-29	Thessaloniki, Greece	3.9 K	Founda et al. (2007)
2006-03-29	Thission (Athens), Greece	2.6 K	Founda et al. (2007)
2006-03-29	Athens, Greece	0.7 K	Tzanis et al. (2008)
2006-03-29	Ibadan, Nigeria	2.2 K	Economou et al. (2008)
2008-08-01	Svalbard, Norway	0.3–1.5 K	Sjöblom (2010)
2010-01-15	Gadanki, India, –0.10 m	3.0 K	Venkat Ratnam et al. (2010)
2010-01-15	Gadanki, India, –0.20 m	1.3 K	Venkat Ratnam et al. (2010)
2010-01-15	Gadanki, India, 0.00 m	5.4 K	Venkat Ratnam et al. (2010)
2010-01-15	Gadanki, India, 0.05 m	5.0 K	Venkat Ratnam et al. (2010)
2010-01-15	Gadanki, India, 12 m	2.5 K	Venkat Ratnam et al. (2010)
2010-01-15	Gadanki, India, 4 m	5 K	Venkat Ratnam et al. (2010)
2010-01-15	Gadanki, India, 8 m	3 K	Venkat Ratnam et al. (2010)
2010-01-15	Gadanki, India, surface	5.8 K	Venkat Ratnam et al. (2010)

Date	Where | Additional Information	Temperature Drop	Reference
2010-01-15	Kanyakumari, India	4 K	Murthy et al. (2013)
2010-01-15	Ramanathapuram, India	1 K	Murthy et al. (2013)
2010-01-15	Thiruvananthapuram, India	1.2 K	Bala Subrahamanyam and Anurose (2011)
2010-01-15	Thiruvananthapuram, India, over cassava	4 K	Murthy et al. (2013)
2010-01-15	Thrissur, India	2 K	Murthy et al. (2013)
2010-01-15	Thumba, India	2 K	Murthy et al. (2013)
2010-01-15	Thumba, India	1.2 K	Bala Subrahamanyam et al. (2012)
2010-01-15	Tirunelveli, India	3.2 K	Murthy et al. (2013)
2015-03-20	Mainland UK, maximum drop (of 266 sites)	4.23 K	Clark (2016)
2015-03-20	Mainland UK, median drop (of 266 sites)	1.02 K	Clark (2016)
2015-03-20	Mainland UK, minimum drop (of 266 sites)	0.03 K	Clark (2016)
2015-03-20	Mainland UK, mean drop (of 76 sites)	0.83 ± 0.63 K	Hanna et al. (2016)
2015-03-20	Mainland UK, mean drop, clear sky (14 sites)	0.91 ± 0.78 K	Hanna et al. (2016)
2015-03-20	Mainland UK, mean drop, cloudy sky (16 sites)	0.31 ± 0.40 K	Hanna et al. (2016)
2015-03-20	Svalbard, Norway	0.3–1.5 K	Pasachoff et al. (2016)
2015-03-20	Switzerland, 184 stations	1.5 K	*This study*
2015-03-20	Sorniot–Lac Inférier (Switzerland, most extreme drop)	5.8 K	*This study*

Table 2. Fitting parameters of gamma distribution (Eq. 4) fitted to empirical histograms of temperature drops ΔT during the eclipses and mean ΔT. All values are best estimates $\pm$ standard error of the estimate. Values in italics indicate that the parameter estimates were not significantly different from zero ($p > 0.05$).

	Offset (K)	Shape	Scale	mean ΔT (K)
This study	-1.1 ± 0.3	6.6 ± 1.9	0.4 ± 0.1	1.5 ± 1.0
Literature data	*–3.5 ± 3.1*	*12.8 ± 13.1*	*0.5 ± 0.3*	2.6 ± 1.7
Combined	-0.7 ± 0.1	3.4 ± 0.4	0.8 ± 0.1	1.9 ± 1.4

Table 3. ~~Probabilities~~ Empirical probabilities Pr($\leq \Delta$T) ~~deduced from Table 2~~ to relate a future temperature drop during an eclipse to values previously published in the literature and in this paper. Bold figures are above the median, and figures in italics are below the 10% percentile of the empirical probability distribution. The sign convention uses ~~negative~~ positive ΔT if temperature gets colder during the occulation phase.

ΔT (K)	All	Literature	This study
~~−2.0~~ 11.0	~~>~~**~~0.999~~** *<0.001*	~~>~~**~~0.999~~** *<0.001*	~~>~~**~~0.999~~** *<0.001*
~~−1.5~~ 10.5	~~>~~**~~0.999~~** *0.003*	**~~0.999~~** *0.008*	~~>~~**~~0.999~~** *<0.001*
~~−1.0~~ 10.0	~~>~~**~~0.999~~** *0.003*	**~~0.996~~** *0.008*	~~>~~**~~0.999~~** *<0.001*
~~−0.5~~ 9.5	**~~0.999~~** *0.003*	**~~0.985~~** *0.008*	**~~0.998~~** *<0.001*
~~0.0~~ 9.0	**~~0.967~~** *0.007*	**~~0.958~~** 0.017	**~~0.961~~** *<0.001*
~~0.5~~ 8.5	**~~0.867~~** *0.007*	**~~0.908~~** 0.017	**~~0.838~~** *<0.001*
~~1.0~~ 8.0	**~~0.719~~** 0.013	**~~0.830~~** 0.033	**~~0.644~~** *<0.001*
~~1.5~~ 7.5	**~~0.558~~** 0.016	**~~0.729~~** 0.041	~~0.438~~ *<0.001*
~~2.0~~ 7.0	~~0.412~~ 0.020	**~~0.613~~** 0.050	~~0.268~~ *<0.001*
~~2.5~~ 6.5	~~0.292~~ 0.023	~~0.494~~ 0.058	~~0.150~~ *<0.001*
~~3.0~~ 6.0	~~0.200~~ 0.030	~~0.381~~ 0.074	~~0.078~~ *<0.001*
~~3.5~~ 5.5	~~0.134~~ 0.036	~~0.283~~ 0.083	~~0.038~~ *0.005*
~~4.0~~ 5.0	~~0.087~~ 0.056	~~0.202~~ 0.116	~~0.018~~ 0.016
4.5	~~0.056~~ 0.085	~~0.139~~ 0.182	~~*0.008*~~ 0.022
~~5.0~~ 4.0	~~0.035~~ 0.108	~~0.093~~ 0.223	~~*0.003*~~ 0.033
~~5.5~~ 3.5	~~0.022~~ 0.151	~~0.060~~ 0.289	~~*0.001*~~ 0.060
~~6.0~~ 3.0	~~0.014~~ 0.203	~~0.038~~ 0.372	~~*0.001*~~ 0.092
~~6.5~~ 2.5	~~*0.008*~~ 0.292	~~0.023~~ **0.521**	~~*<0.001*~~ 0.141
~~7.0~~ 2.0	~~*0.005*~~ 0.420	~~0.014~~ **0.653**	~~*<0.001*~~ 0.266
~~7.5~~ 1.5	~~*0.003*~~ **0.567**	~~*0.008*~~ **0.736**	~~*<0.001*~~ 0.457
~~8.0~~ 1.0	~~*0.002*~~ **0.721**	~~*0.005*~~ **0.835**	~~*<0.001*~~ **0.647**
~~8.5~~ 0.5	~~*0.001*~~ **0.872**	~~*0.003*~~ **0.917**	~~*<0.001*~~ **0.842**
~~9.0~~ 0.0	~~*0.001*~~ **0.970**	~~*0.001*~~ **0.967**	~~*<0.001*~~ **0.973**
~~9.5~~ −0.5	~~*<0.001*~~ >**0.999**	~~*0.001*~~ >**0.999**	~~*<0.001*~~ >**0.999**
~~10.0~~ −1.0	~~*<0.001*~~ >**0.999**	~~*<0.001*~~ >**0.999**	~~*<0.001*~~ >**0.999**
~~10.5~~ −1.5	~~*<0.001*~~ >**0.999**	~~*<0.001*~~ >**0.999**	~~*<0.001*~~ >**0.999**
~~11.0~~ −2.0	~~*<0.001*~~ >**0.999**	~~*<0.001*~~ >**0.999**	~~*<0.001*~~ >**0.999**